

https://dspace.org/

Two Higgs-doublet models in future ep colliders

Mosomane, Chuene Johannes

2018

https://hdl.handle.net/10539/26037

Mosomane, Chuene Johannes (2018) Two Higgs-doublet models in future ep colliders, University of the Witwatersrand, Johannesburg, https://hdl.handle.net/10539/26037

Downloaded from a DSpace repository. https://dspace.org/



University of the Witwatersrand

A dissertation submitted in the fulfilment of the requirement for the Master of Science in the school of physics

Two Higgs-doublet models in future $e^{-}p$ colliders

Author:
Mr. Chuene Mosomane

Supervisors:
Prof. Alan Cornell
Dr. Deepak Kar

Abstract

We review the general two Higgs doublet model and its particle spectrum. This model has four types, which are Type-I, Type-II, Type-X (lepton specific) and Type-Y (Flipped). We discuss the Madala hypothesis as a Type-II two Higgs doublet model, where the Madala hypothesis introduces the Madala boson (which is a doublet-like heavy Higgs boson) with $m_H = 270$ GeV. We study the Madala boson in the proposed LHeC, which is a ep collider. The Madala boson has a higher cross-section in the LHeC with proton beam energy of $E_p = 7$ TeV in the charge current and the neutral current is suppressed.

Declaration

I, the undersigned, hereby declare that the work contained in this dissertation is my original work and that any work done by others or by myself previously has been acknowledged and referenced according to the requirement of the Faculty of Science of the University of the Witwatersrand.

Signed:



_____

Date:
16 March 2018

_____

Preface

The contents of this dissertation are based on the following published paper and presented conference proceedings:

Paper:

- Chuene Mosomane, Mukesh Kumar, Alan S. Cornell and Bruce Mellado "Exploring CP-even scalars of Two Higgs-doublet model in the future $e^{-}p$ colliders" in preparation [1].

Proceedings:

- Chuene Mosomane "Two Higgs-doublet models in the future colliders" J. Phys. Conf. Ser. 889 (2017) 012004, `arXiv:1707.05997 [hep-ph]` [1].
- Chuene Mosomane "Two Higgs-doublet models and the LHC" Proceedings of SAIP 2016, ISBN: 978-0-620-77094-1.

Acknowledgements

This dissertation would not have been possible without the support of several people. Firstly I would like to thank my supervisor, Prof Alan Cornell for dedicating his time and his patience to me. I would also like to thank Dr Mukesh Kumar, for his unlimited patience and being my tutor, I really learned a lot from him. and also I would like to thank Prof Robert de Mello Koch for his Quantum Field Theory lectures.

I greatly thank the professors who will patiently read this work.

I would like to give special thanks to my family for their support and patience, and my office mate (Mohammed Khojali) and friends for the endless discussions about physics, and creating a great and conducive environment.

Lastly, I would like to thank the NRF, which gave me funding for this dissertation.

Contents

Abstract i

Declaraton ii

Preface iii

Acknowledgements iv

1 Introduction 1

2 The Standard Model 3

2.1 Gauge symmetry . . . 4

2.1.1 Global symmetry . . . 5

2.1.2 Local symmetry . . . 5

2.1.3 Mass matrix and the Goldstone theorem . . . 7

2.2 Electroweak Theory . . . 8

2.2.1 Spontaneous symmetry breaking . . . 8

2.3 Yukawa sector in the Standard Model . . . 11

2.4 Summary . . . 15

3 Two Higgs-doublet models 16

3.1 Motivation . . . 16

3.2 The Scalar sector . . . 17

3.3 The Yukawa interaction . . . 22

3.3.1 Branching of the scalars in 2HDM . . . 24

3.4 The Madala Hypothesis . . . 30

4 Constraints on the 2HDM 33

4.1 Theoretical Constraints . . . 33

4.2 Experimental Constraints . . . 34

4.3 Collider Constraints . . . 35

4.3.1 Large Hadron Collider . . . 38

4.3.2 2HDM CP-even scalars study in the LHC 39
4.3.3 International Linear Collider 41

5 The Large Hadron electron Collider 43
5.1 Electron-Proton Scattering 44
5.1.1 Elastic Scattering 46
5.1.2 Inelastic scattering 47
5.2 Detector 50

6 Exploring two CP-even scalars in the LHeC 51
6.1 Production of the Madala boson in the LHeC 51
6.2 Discussion 53

7 Conclusion 57

A Branching ratio 59

B Parton distribution functions 62

C Scattering Amplitude 64

Chapter 1

Introduction

The theoretical starting point of particle physics is the Standard Model (SM), where we are living in the new era post the discovery of the Higgs boson, which has opened up many new opportunities. Note that the SM was developed in the late 20th century by Glashow, Weinberg and Salam [2], and the Higgs boson was discovered in 2012 [3], as the last missing piece of the SM. Furthermore, recall that the SM allows us to calculate the interactions between fundamental particles with a high degree of accuracy. And this is the reason why the Higgs boson is important in the SM, as it is responsible for how fundamental particles acquire mass, and it makes the model renormalisable. In the SM the Higgs sector consists of one complex Higgs doublet field, which allows the Higgs mechanism to be possible, and as a result the Higgs mechanism leads to electroweak symmetry breaking (EWSB) generating the masses of the gauge bosons and fermions through the Yukawa interactions.

One of the successful achievements of particle physics is building particle colliders, which serve in the search of these fundamental particles, and the validation of the Higgs boson. These colliders run at a very high energy scales, at which they collide particles like protons or electrons together. There are different types of colliders, where all of them have their own significance. To speak of a few, the Large Hadron Collider (LHC) collides protons together, where at run-I the energy scale was $7-8$ TeV, and run-II which will be $13-14$ TeV; the International Linear Collider (ILC) collides leptons (electrons and positrons) together at 500 GeV to 1 TeV [4].

However, despite the great successes of the SM in explaining much of the available data, it cannot be the last answer, as it has some inadequacies and also there are phenomenological indications that the SM cannot answer. For example the SM doesn't account for the baryonic number of particles, it doesn't include gravity, and

doesn't talk about the dark matter in the universe. These are some of the reasons that lead particle physicists to go beyond the SM (BSM) [5], where there are many theories that explain these phenomena, such as supersymmetry, extra dimensions, technicolour, etc. In this dissertation we shall look at the general two Higgs doublet model (2HDM) [6]. This model has an extended Higgs sector, and is a simple extension of the SM, where we add an extra scalar doublet to the SM.

The motivation behind this framework comes from the breaking of the electroweak symmetry in the SM and asking why this only gives rise to one scalar field. By adding another scalar doublet we observe some interesting properties, such as the production of additional Higgs particles, sources of CP-violation and flavour changing neutral currents (FCNCs). A discrete symmetry can be introduced to the Yukawa sector, which splits the 2HDM into four different types, see section 3.3 [6]. The 2HDM provides us with the opportunity to solve the CP-violation problem, which is responsible for generating the observed matter-antimatter asymmetry in the universe [7]. Recall that it is not possible to generate baryon number in the SM, because it has a small amount of CP-violation (via the CKM matrix). In this work CP-conservation is important and we shall only consider decays where it is conserved. Collider experiments provide us with a tool to validate the frameworks with the available data, with various experiments, such as the LHC and Tevatron and the ILC. In this dissertation we shall concentrate in the Large Hadron electron Collider (LHeC), which shall collide electrons and protons together. The reason why we look at this collider environment in particular is because we want to study the CP-even scalar particles of the 2HDM. The study of deep inelastic scattering has been known to be an important tool in particle physics as it helps with the study of the structure of the proton in a more fundamental way, such as understanding gives us an picture of how protons are made up of quarks, which are confined. In this dissertation we shall start by elastic scattering as a preliminary study, and then continue with the study of the deep inelastic scattering.

With this in mind, this dissertation shall be structured as follows: In the second chapter we introduce the SM and how spontaneous symmetry breaking plays a significant role in the production of massive elementary particles. Building on this theory we focus on the scalar sector only, as it is important to us in studying the CP-even scalars in the 2HDM. The SM acts as a stepping stone to talking about the 2HDM in the third chapter. In this chapter we start by building the 2HDM scalar sector, we shall do that by adding an extra scalar doublet to the SM, then we

shall also talk about the Yukawa interactions. Writing down the full Lagrangian of the 2HDM, we then apply spontaneous symmetry breaking and obtain five different scalar particles. Looking at the Yukawa interactions we end up with different types of models, which we shall explicitly mention at the end of chapter 3. Applying a specific choice of parameters to the scalar sector for the CP-even scalars, we shall link this to the Madala hypothesis (postulate a new heavy scalar, H which explains several independent anomolous features seen in the ATLAS and CMS data) [8] which is relevant to our study. We also look at constraints on the 2HDM in the fourth chapter, which shall show how our frameworks are constrainted theoretically and experimentally. We also talk about different colliders, such as the LHC and the ILC in chapter four. In chapter five we talk about the LHeC and the scattering processes (elastic and inelastic scattering), and chapter six we focus on the LHeC and how we could observe the Madala boson, looking at two different scattering processes. We shall mainly study the heavy scalar boson (the Madala boson), its production rate and branching ratios, by comparing it to the lightest scalar boson, which we identify as the SM-like Higgs boson. Chapter seven shall be a presentation of our future possible work and conclusions.

Chapter 2

The Standard Model

The SM is a theoretical framework which uses the language of quantum field theory (QFT) to explain how fundamental particles such as (quarks and leptons) interact with each other. The SM is considered to be an effective theory at a low energy scale which may be superseded by a model BSM at a higher energy scale. The interactions are mediated by gauge bosons, which in the SM are the photons (which carry information on the electromagnetic force), the vector bosons ($W^{\pm}, Z^{0}$, which are the carriers of the weak force), and the gluons (the strong force); these being the forces described by the SM. The Higgs boson in the SM has been confirmed by the CMS and ATLAS experiments at CERN through run-I data [3, 9], completing the SM particle spectrum.

Particle physics addresses the questions of what are the building blocks of matter, and what are the fundamental laws that govern our universe. The fundamental particles come in bosons and fermions, where the fermions are divided into three generations. The first generation are the lightest particles, and the third generation are the heaviest particles. These fermions are grouped further into quarks (which form the constituents of mesons and hadrons) and the leptons (such as electrons, neutrinos, etc.) These fermions interact with each other through the mediation of gauge bosons, which are also referred to as force carriers. These particles acquire mass by introducing a Higgs mechanism through EWSB (see section 2.2.1 for more details).

The fermions have spin-1/2 and obey the Pauli exclusion principle. The fermions are divided into quarks and leptons, where there are six quarks; up, down, charm, strange, top and bottom, carrying both electric and colour charge. Furthermore, there are also six leptons; electron, muon, tauon, electron neutrino, muon neutrino,

tauon neutrino. The electron, muon and tauon carry electric charge, whereas the remaining three neutrinos carry no charge at all. All leptons and quarks carry weak hypercharge, allowing them to interact with the gauge bosons of the weak interaction, the $W^{\pm}$ and Z bosons. Neutrinos only interact via the weak interaction and often appear as missing energy in colliders. Because the electron, muon and tauon have electric charge they can interact via the exchange of photons. The quarks also

Table 2.1: *A summary of the SM fermion content and their quantum numbers, where* $i = 1, 2, 3$

Fields	Parity	$SU(3)_c$	$SU(2)_L$	$U(1)_Y$
Q_L^i	L	3	2	1/6
u_R^i	R	3	1	2/3
d_R^i	R	3	1	-1/3
L_L^i	L	1	2	-1/2
e_R^i	R	1	1	-1

carry electric charge and colour, and are never free, that is, they are always observed at low energies in bound states (a phenomena called confinement). In recent years high-energy experiments have confirmed the SM in many ways, for example, the top quark was theoretically predicted in the middle twentieth century, but it took 18 years to produce and detect it in the Tevatron [10]. Even though the experiments verify many aspects of the SM, it is not a complete theory of nature, since several questions remain unanswered such, as those mentioned in the introduction chapter.

2.1 Gauge symmetry

The first time many people encounter gauge theories is in electrodynamics courses, where Maxwell's equation obey a $U(1)$ gauge transformation. The reason we are interested in gauge theories is that they can describe the fundamental forces of nature, such as electromagnetism, the weak force and the strong force. We shall make no statement about the force of gravity. These fundamental forces have been described in the SM, which is a non-Abelian gauge theory with a symmetry group $SU(3)_c \times SU(2)_L \times U(1)_Y$. The $SU(3)_c$ group, with c standing for the colour charge, is a group for strong interactions and is a representation for Quantum ChromoDynamics (QCD). QCD describes the interactions between quarks via the exchange of gluons, which are massless, come in eight varieties and interact with quarks. The $SU(2)_L$ group, with L standing for left-handed doublet, is the group for the weak interactions. The $U(1)_Y$ group is for hypercharge, with Y standing for hypercharge. The unification of the weak interactions and electromagnetism forms a group $SU(2)_L \times U(1)_Y$, which is the electroweak symmetry group. This $SU(2)_L \times U(1)_Y$

breaks, via the Higgs mechanism, to the $U(1)_{em}$ of electromagnetism (see section 2.2.1).

To construct sucha theory, first recall that a gauge theory is a theory where the action, or equations of motion, become invariant under a continuous symmetry that depends on space-time. There are two symmetries that we are concerned with, global symmetries and local symmetries. Note that Global symmetry does not depend on space-time co-ordinates, whereas local symmetries do depend on space-time co-ordinates.

2.1.1 Global symmetry

Let us consider a field $\psi(x)$ with a constant phase α which transforms as follows:

$$\psi(x) \to \psi'(x) = e^{i\alpha}\psi(x), \tag{2.1}$$

$$\bar{\psi}(x) \to \bar{\psi}'(x) = e^{-i\alpha}\bar{\psi}(x). \tag{2.2}$$

As a simple case, a Lagrangian that is invariant under this global transformation is the Dirac's Lagrangian for a free fermionic field:

$$\begin{aligned} \mathcal{L} &= \bar{\psi}(x)(i\gamma^\mu\partial_\mu - m)\psi(x) \\ &= e^{-i\alpha}\bar{\psi}(x)(i\gamma^\mu\partial_\mu - m)e^{i\alpha}\psi(x) \\ &= \bar{\psi}(x)(i\gamma^\mu\partial_\mu - m)\psi(x) \\ &= \mathcal{L}. \end{aligned} \tag{2.3}$$

That is, the Lagrangian is invariant under a constant phase shift.

2.1.2 Local symmetry

For a local symmetry the phase is a function of space-time, $\alpha(x)$, and the field $\psi(x)$ transforms as:

$$\psi(x) \to \psi'(x) = e^{i\alpha(x)}\psi(x), \tag{2.4}$$

$$\bar{\psi}(x) \to \bar{\psi}'(x) = e^{-i\alpha(x)}\bar{\psi}(x). \tag{2.5}$$

We start by making the local $U(1)$ transformation on the Dirac Lagrangian:

$$\begin{aligned}\mathcal{L} &= \bar{\phi}(x)(i\gamma^\mu\partial_\mu - m)\psi(x) \\ &= e^{-i\alpha(x)}\bar{\psi}(x)(i\gamma^\mu\partial_\mu - m)e^{i\alpha(x)}\psi(x).\end{aligned} \tag{2.6}$$

But now the differential operators act on $\alpha(x)$ as well as $\phi(x)$, and we get an extra term:

$$\begin{aligned}\mathcal{L} &= \bar{\psi}(x)e^{-i\alpha(x)}(i\gamma^\mu\partial_\mu - m)e^{i\alpha(x)}\psi(x) \\ &= \bar{\psi}(x)e^{-i\alpha(x)}(i\gamma^\mu\partial_\mu - m)\psi(x)e^{i\alpha(x)} - \bar{\psi}(x)e^{-i\alpha(x)}\gamma^\mu\psi(x)e^{i\alpha(x)}\partial_\mu\alpha(x) \\ &= \bar{\psi}(x)(i\gamma^\mu\partial_\mu - m)\psi(x) - \bar{\psi}(x)\gamma^\mu\psi(x)\partial_\mu\alpha(x).\end{aligned} \tag{2.7}$$

To demand that $\mathcal{L}$ be invariant under this local $U(1)$ transformation, we should find a way to cancel the $\bar{\psi}(x)\gamma^\mu\psi(x)\partial_\mu\alpha(x)$ term. To do that we define a new field A_μ, which under the local $U(1)$ transformation transforms according to:

$$A_\mu \to A_\mu - \frac{1}{q}\partial_\mu\alpha(x). \tag{2.8}$$

By defining the A_μ to transform this way, where we call A_μ the gauge field and q is a constant, means we can introduce the A_μ by replacing the standard derivative operator ∂_μ, with the covariant derivative

$$D_\mu = \partial_\mu + iqA_\mu. \tag{2.9}$$

The Lagrangian now becomes:

$$\begin{aligned}\mathcal{L} &= \bar{\psi}(x)(i\gamma^\mu D_\mu - m)\psi(x) \\ &= \bar{\psi}(x)(i\gamma^\mu[\partial_\mu + iqA_\mu] - m)\psi(x) \\ &= \bar{\psi}(x)(i\gamma^\mu\partial_\mu - q\gamma^\mu A_\mu - m)\psi(x).\end{aligned} \tag{2.10}$$

Under the $U(1)$ transformation we have:

$$\begin{aligned}\mathcal{L} &= \bar{\psi}(x)e^{-i\alpha(x)}(i\gamma^\mu\partial_\mu - q\gamma^\mu[A_\mu - \frac{1}{q}\partial_\mu\alpha(x)] - m)e^{i\alpha(x)}\psi(x) \\ &= \bar{\psi}(x)(i\gamma^\mu\partial_\mu - q\gamma^\mu A_\mu - \gamma^\mu\partial_\mu\alpha(x) + \gamma^\mu\partial_\mu\alpha(x) - m)\psi(x) \\ &= \bar{\psi}(x)(i\gamma^\mu\partial_\mu - q\gamma^\mu A_\mu - m)\psi(x) \\ &= \bar{\psi}(x)(i\gamma^\mu D_\mu - m)\psi(x) \\ &= \mathcal{L}.\end{aligned} \tag{2.11}$$

The field A_μ has restored the local $U(1)$ symmetry, and we notice that it is also invariant under the global $U(1)$ which we had started with. Note the conserved current $j^\mu = \bar{\psi}(x)\gamma^\mu\psi(x)$. The Lagrangian has become:

$$\begin{aligned}\mathcal{L} &= \bar{\psi}(x)(i\gamma^\mu D_\mu - m)\psi(x) \\ &= \bar{\psi}(x)(i\gamma^\mu\partial_\mu - m)\psi(x) - qj^\mu A_\mu.\end{aligned} \tag{2.12}$$

Note that when we take the variation of the A_μ the current vanishes, we get the following,

$$\begin{aligned}\frac{\partial\mathcal{L}}{\partial A_\mu} &= -q\bar{\psi}(x)\gamma^\mu\psi(x) \\ &= -qj^\mu \\ &= 0.\end{aligned} \tag{2.13}$$

To obtain a dynamical gauge field, the Lagrangian density needs to be completed by a term that describes the dynamic behaviour of the gauge field. This term should be gauge and Lorentz covariant, which is true for the square of the field strength tensor, defined as:

$$\mathcal{L}_{kin} = -\frac{1}{4}F_{\mu\nu}F^{\mu\nu}, \tag{2.14}$$

where

$$F^{\mu\nu} = \partial^\mu A^\nu - \partial^\nu A^\mu. \tag{2.15}$$

Therefore, the Lagrangian becomes, where we include a dynamical gauge field:

$$\mathcal{L}_{QED} = \bar{\psi}(x)(i\gamma^\mu D_\mu - m)\psi(x) - \frac{1}{4}F_{\mu\nu}F^{\mu\nu}. \tag{2.16}$$

Because A_μ is a physical field, we can also assume that there is some source term, which is j^μ. The final Lagrangial becomes

$$\mathcal{L} = \bar{\psi}(x)(i\gamma^\mu D_\mu - m)\psi(x) - \frac{1}{4}F_{\mu\nu}F^{\mu\nu} - J^\mu A_\mu. \tag{2.17}$$

This is the Lagrangian that describes quantum electrodymanics.

2.1.3 Mass matrix and the Goldstone theorem

The observation that massless particles appear in theories with spontaneously broken continuous symmetries is a general result known as Goldstone's theorem [11] . The first example for such particles was suggested by Nambu in 1960 [12]. He showed that a massless quasi-particle appears in a magnetised solid, because the magnetic field breaks rotational invariance. Goldstone applied this idea shortly afterwards to relativistic QFTs, and showed that massless scalar particles appear in theories with spontaneous symmery breaking. Since no massless scalar particles are known to exist, this theorem appeared to be a dead end for the application of spontaneous symmetry breaking to particle physics. However, what if our spontaneously broken symmetry were a gauge symmetry?

The Goldstone theorem has important consequences for spontaneous symmetry breaking:

- The Lagrangian remains invariant, but the state of minimal energy, the vacuum state, is no longer invariant. As the excited states are obtained from the action of generators on the vacuum, the symmetry is no longer manifest in the spectrum of the states.
- There exist some physical massless states whose properties are connected to those of generators of the broken symmetry. These are the Goldstone bosons. There are as many Goldstone bosons as there are broken generators.

We shall now illustrate another formulation of this theorem by considering a theory involving several scalar fields $\psi_i(x)$, defining the Lagrangian as the difference between K, the kinetic energy and V, potential energy:

$$\mathcal{L} = K - V(\phi). \tag{2.18}$$

If we expand V about the minimum, we get:

$$V(\phi) = V(\phi_0) + \frac{\partial V(\phi_0)}{\partial \phi_i}\phi_i' + \frac{1}{2}\frac{\partial^2 V(\phi_0)}{\partial \phi_i \partial_j}\phi_i'\phi_j' + ..., \tag{2.19}$$

where the ϕ_0 are the constant fields that minimise V, such that

$$\left(\frac{\partial V}{\partial \phi_i}\right)_{\phi_i=\phi_0} = 0. \tag{2.20}$$

These constant fields minimise the Hamiltonian and the energy, thus they define the vacuum state.

If we redefine the fields:

$$\varphi_i(x) = \phi_i(x) - \phi_{0,i},$$

and call the quadratic term the mass matrix:

$$m_{ij}^2 = \frac{\partial^2 V(\phi_0)}{\partial \phi_i \partial \phi_j}, \tag{2.21}$$

this matix is symmetric because derivatives commute, and has eigenvalues that give the masses of the fields. The masses are always positive or null, since ϕ_0 is a minimum. Each continuous symmetry of $\mathcal{L}$ that is not a symmetry of ϕ_0 gives rise to a zero eigenvalue of this mass matrix. This is another formulation of the Goldstone theorem, which states that for every spontaneoussly broken continuous symmetry, a massless particle appears.

However, in the SM, the Lagrangian posseses a local gauge symmetry. Therefore, the consequences of the symmetry breaking is that Goldstone bosons become new longitudinal polarisation states of the gauge bosons, the latter becoming massive and the former disappear from the spectrum, as we shall review in the next section.

2.2 Electroweak Theory

2.2.1 Spontaneous symmetry breaking

We shall study the local $SU(2)_L \times U(1)_Y$ gauge invariance, which shall lead us to breaking the symmetry of this theory by keeping the full Lagrangian invariant under $SU(2)_L \times U(1)_Y$ and the vacuum not invariant under this symmetry. This is done by introducing a new doublet, which is the Higgs field, and has four degrees of freedom.

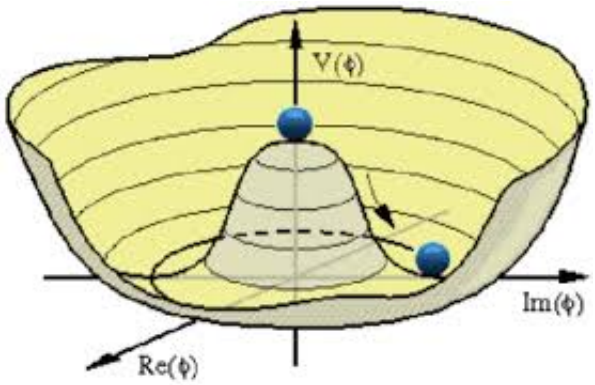

Figure 2.1: *Mexican hat Higgs potential of the SM*

Three degrees of freedom shall be absorbed as the longitudinal degrees of freedom, and shall generate masses for the gauge bosons ($W^{\pm}, Z^0$). The other degree of freedom is the photon, which remains massless. The process of breaking the symmetry and making the gauge boson massive is called the Higgs mechanism [13].

Introducing the complex doublet scalar field:

$$\phi = \begin{pmatrix} \phi^+ \\ \phi^0 \end{pmatrix} = \frac{1}{\sqrt{2}} \begin{pmatrix} \phi_1 + i\phi_2 \\ \phi_3 + i\phi_4 \end{pmatrix}, \tag{2.22}$$

we start by writing down the Lagrangian of the scalar field as:

$$\mathcal{L}(\phi^\dagger\phi) = (D^\mu\phi)^\dagger(D_\mu\phi) - V(\phi^\dagger\phi). \tag{2.23}$$

The covariant derivative takes the form:

$$D_\mu = \partial_\mu - igW_\mu^a T_a - ig'\frac{1}{2}B_\mu Y, \tag{2.24}$$

with $T_a = \sigma^a/2$, σ^a (where $a = 1, 2, 3, ...$) being the Pauli matrices which are the generators of $SU(2)_L$ in the fundamental representation, and Y is the hypercharge, the generators of $U(1)_Y$.

The potential has the form:

$$V(\phi^\dagger\phi) = \mu^2(\phi^\dagger\phi) + \lambda(\phi^\dagger\phi)^2, \tag{2.25}$$

μ^2 being the mass term of the scalar field, which develops a nonzero vacuum expectation value (vev) for $\mu^2 < 0$ and $\lambda > 0$. The λ term is the quartic self-interations among the scalar fields. Note that vacuum stability demands $\lambda > 0$. Since the

potential depends on the combination of the $(\phi^\dagger\phi)$, it obtains a minimum [14]

$$\langle 0|\phi_0|0\rangle = \begin{pmatrix} 0 \\ \frac{v}{\sqrt{2}} \end{pmatrix}. \tag{2.26}$$

Owing to the conservation of the electric charge, only a neutral scalar can acquire a vev. Thus, with the choice above, ϕ^0 is to be interpreted as the neutral component of the doublet as $Q(\phi) = I_{3w} + \frac{1}{2}y = 0$, that is, electromagnetism is unbroken by the scalar vev. The components I_{3w} are the $SU(2)$ doublet third component of isospin and take on values $\pm 1/2$. The term $y/2$ are the hypercharge assignments.

For convenienece, we thus write the scalar doublet in a unitary gauge as follows [14]:

$$\langle 0|\phi_0|0\rangle = \exp\left(\frac{i\zeta^a(x)\sigma^a}{v}\right)\begin{pmatrix} 0 \\ \frac{v+h(x)}{\sqrt{2}} \end{pmatrix}. \tag{2.27}$$

The exponential form corresponds to the gauge rotations. We have introduced the fields $\zeta^a(x)$ and $h(x)$, where the $\zeta^a(x)$ acts on the doublet to repopulate the fields ϕ_1, ϕ_2, ϕ_4, and we can reparametrise these components such tha the Goldstone boson absorbs the gauge bosons, to make a massive Higgs field, $h(x)$.

After a gauge transformation

$$U(1)_Y : \phi \to \exp\left[i\alpha(x)\cdot\frac{1}{2}\right]\phi,$$
$$SU(2)_L : \phi \to \exp\left[i\alpha^a(x)\cdot\frac{\sigma^a}{2}\right]\phi,$$

with $\alpha^a(x) = \dfrac{-\zeta^a(x)}{v} \implies \phi = \begin{pmatrix} 0 \\ \frac{v+h(x)}{\sqrt{2}} \end{pmatrix}$.

For the gauge-kinetic term we substitute the covariant derivative, the Pauli matrices and the hypercharge: Pauli matices and the hypercharge are defined as follows [14];

$$\sigma^1 = \begin{pmatrix} 0 & 1 \\ 1 & 0 \end{pmatrix}, \qquad \sigma^2 = \begin{pmatrix} 0 & -i \\ i & 0 \end{pmatrix}, \qquad \sigma^3 = \begin{pmatrix} 1 & 0 \\ 0 & -1 \end{pmatrix}, \tag{2.28}$$

$$Y = \begin{pmatrix} 1 & 0 \\ 0 & 1 \end{pmatrix}, \tag{2.29}$$

$$\implies D_\mu\phi = \frac{1}{\sqrt{2}}\begin{pmatrix} -i\frac{g}{2}(W_\mu^1 - iW_\mu^2)(v+h) \\ \partial_\mu h + \frac{i}{2}(-g'B_\mu + gW_\mu^3)(v+h) \end{pmatrix}. \tag{2.30}$$

Multipying with the hermitian conjugate term we get the following expression;

$$\begin{aligned}(D_\mu\phi)^\dagger(D^\mu\phi) =& \frac{1}{2}(\partial_\mu h)(\partial^\mu h) + \frac{1}{8}(v+h)^2(-g'B_\mu + gW_\mu^3)(-g'B_\mu + gW_\mu^3) \\ &+ \frac{1}{8}g^2(v+h)^2(W_\mu^1 - iW_\mu^2)(W_\mu^1 + iW_\mu^2).\end{aligned} \tag{2.31}$$

After the expansion of the $(v+h)^2$, the second and the third terms become:

$$\frac{v^2}{8}(g'B_\mu - gW_{3\mu})(g'B^\mu - gW_\mu^3) \equiv \frac{1}{2}m_Z^2 Z_\mu Z^\mu + \frac{1}{2}\times 0 \times A_\mu A^\mu. \tag{2.32}$$

The Z_μ is the massive linear combination of the $W_{3\mu}$ and B_μ. The A_μ is a massless linear combination of the W_μ^3 and B_μ.

In a matrix form this becomes:

$$\frac{1}{2}\begin{pmatrix} Z_\mu, A_\mu \end{pmatrix}\begin{pmatrix} m_Z^2 & 0 \\ 0 & 0 \end{pmatrix}\begin{pmatrix} Z^\mu \\ A^\mu \end{pmatrix} \equiv \frac{v^2}{8}\begin{pmatrix} W_{3\mu}, B_\mu \end{pmatrix}\begin{pmatrix} g^2 & -g'g \\ -g'g & g'^2 \end{pmatrix}\begin{pmatrix} W_3^\mu \\ B^\mu \end{pmatrix} \tag{2.33}$$

$$\implies \begin{pmatrix} Z^\mu \\ A^\mu \end{pmatrix} = \begin{pmatrix} \cos\theta_w & -sin\theta_w \\ \sin\theta_w & \cos\theta_w \end{pmatrix}\begin{pmatrix} W_3^\mu \\ B^\mu \end{pmatrix}. \tag{2.34}$$

We define $Z_\mu = \cos\theta_w W_\mu^3 - \sin\theta_w B_\mu$ and $A_\mu = \sin\theta_w W_\mu^3 + \cos\theta_w B_\mu$,

where $\cos\theta_w = \dfrac{g'}{\sqrt{g^2+g'^2}}$ and $\sin\theta_w = \dfrac{g}{\sqrt{g'^2+g^2}}$.

Note that the introduced angle, θ_w, is the Weinberg angle. The mass of the Z-boson is [14]

$$m_Z^2 = \frac{v^2}{4}(g^2+g'^2). \tag{2.35}$$

The third term in Eqn. (2.31) becomes:

$$\frac{g'^2v^2}{2}(W_{1\mu} - iW_{2\mu})(W_1^\mu + iW_2^\mu) \equiv m_W^2 W_\mu^+ W^{-\mu}, \tag{2.36}$$

where $W_\mu^\pm = \frac{1}{\sqrt{2}}(W_{1\mu} \mp iW_{2\mu})$. The mass of the W-boson is [14],

$$m_W^2 = \frac{1}{4}g'^2v^2. \tag{2.37}$$

The expansion of the potential becomes

$$V(\phi^\dagger\phi) = \mu^2(\phi^\dagger\phi) + \lambda(\phi^\dagger\phi)^2 \tag{2.38}$$

$$= \lambda v^2 h^2 + \lambda v h^3 + \frac{1}{4}\lambda h^4 - \frac{1}{4}\lambda v^2, \tag{2.39}$$

where the mass term for the Higgs boson is $m_h^2 = 2\lambda v^2$.

2.3 Yukawa sector in the Standard Model

The Yukawa Lagrangian entails interactions of fermions with the scalar doublet. For the down-type quark we write the Lagrangian as follows:

$$\mathcal{L}^d_{Yukawa} = iY^d_{ij} Q_i^T \sigma_2 \bar{d}_i \Phi^* + h.c. \tag{2.40}$$

$$= iY^d_{ij} Q_i^T \sigma_2 \bar{d}_i V^*(x) \left(\frac{v+h}{\sqrt{2}}\right) + h.c. \tag{2.41}$$

$$= iY^d_{ij} Q_i'^T \sigma_2 \bar{d}_i \left(\frac{v+h}{\sqrt{2}}\right) + h.c., \qquad Q_i'^T = V^\dagger Q_i, \tag{2.42}$$

using $\bar{d_{Li}} = -\sigma_2 d^*_{Ri}$ and $d_{Ri} = (d_R, s_R, b_R)$, with $(i = 1, 2, 3, ...)$, $Q_i'^T = (d_L, s_L, b_L)$ and V^* is unitary, Y_{ij} (are the complex 3×3 matrices made up of Yukawa couplings). After the spontaneous symmetry breaking give rise to fermionic mass.

Therefore,

$$\mathcal{L}^d_{Yukawa} = \frac{i}{\sqrt{2}}(v+h)(y^d_{11} d^\dagger_R d_L + y^d_{22} s^\dagger_R s_L + y^d_{33} b^\dagger_R b_L) + h.c.. \tag{2.43}$$

So we can define the mass term:

$$\mathcal{M}^d = y^d_{ii}\frac{v}{\sqrt{2}} = (m_d, m_s, m_b). \tag{2.44}$$

We can do the same thing for the leptons, where we have,

$$\mathcal{L}^{e}_{Yukawa} = iY^{d}_{ij} L^{T}_{i} \sigma_2 \bar{e_i} \Phi^{*} + h.c. \tag{2.45}$$

$$= iY^{e}_{ij} L^{T}_{i} \sigma_2 \bar{d}_i U^{*}(x) \left(\frac{v+h}{\sqrt{2}} \right) + h.c. \tag{2.46}$$

$$= iY^{e}_{ij} L'^{T}_{i} \sigma_2 \bar{e_i} \left(\frac{v+h}{\sqrt{2}} \right) + h.c., \qquad L'^{T}_{i} = U^{\dagger} L_i, \tag{2.47}$$

using $\bar{e_{Li}} = -\sigma_2 e^{*}_{Ri}$ and $e_{Ri} = (e_R, \mu_R, \tau_R)$ and $L'^{T}_{i} = (e_L, \mu_L, \tau_L)$, and U^{*} is unitary, Y_{ij} (are the complex 3×3 matrices made up of Yukawa couplings). After the spontaneous symmetry breaking give rise to fermionic mass.

Therefore,

$$\mathcal{L}^{e}_{Yukawa} = \frac{i}{\sqrt{2}} (v+h)(y^{e}_{11} e^{\dagger}_{R} e_L + y^{e}_{22} \mu^{\dagger}_{R} \mu_L + y^{e}_{33} \tau^{\dagger}_{R} \tau_L) + h.c., \tag{2.48}$$

and we can define the mass term:

$$\mathcal{M}^{e} = y^{e}_{ii} \frac{v}{\sqrt{2}} = (m_e, m_\mu, m_\tau). \tag{2.49}$$

The same approach to the up-type quarks is now a little trickier, where we recall that

$$\mathcal{L}^{u}_{Yukawa} = iY^{u}_{ij} Q^{T}_{i} \sigma_2 V_{ji} \bar{u'_j} \tau_2 \Phi + h.c. \tag{2.50}$$

$$= iY^{u}_{ij} Q^{T}_{i} \sigma_2 V_{ji} \bar{u_i} \tau_2 U(x) \left(\frac{v+h}{\sqrt{2}} \right) + h.c. \tag{2.51}$$

using $\tau_2 \tau_i \tau_2 = -\tau^{*}_{i}$ and $\tau_2 U = U^{*} \tau_2 = (U^{\dagger})^{T} \tau_2$, the redefinition $Q' = U^{\dagger} Q_i$ removes the U.

Therefore,

$$\mathcal{L}^{u}_{Yukawa} = i y^{u}_{jj} Q'^{T}_{i} \sigma_2 V_{ji} \bar{u'_j} \tau_2 \frac{v+h}{\sqrt{2}} + h.c., \tag{2.52}$$

where V is the Cabibbo-Kobayashi-Maskawa (CKM) matrix. The mass term is then:

$$\mathcal{M}^{u} = y^{u}_{ii} \frac{v}{\sqrt{2}} = (m_u, m_c, m_t), \tag{2.53}$$

where Yukawa matrices and mass matrices are in general not diagonal in the SM. The next task is to diagonalise the Yukawa matrices to obtain the mass eigenstate. To do that we shall make use of the unitary transformation of the two complex matrices $\mathcal{M}^{u,d}$. Any such matrix can be transformed into a real diagonal matrix by multiplying it on the left and right by appropriate unitary matrices. We define the unitary matrices U_L, U_R, D_L, D_R, such that:

$$\begin{pmatrix} u_1 \\ u_2 \\ u_3 \end{pmatrix}_{L,R} = U_{L,R} \begin{pmatrix} u \\ c \\ t \end{pmatrix}_{L,R}, \qquad \begin{pmatrix} d_1 \\ d_2 \\ d_3 \end{pmatrix}_{L,R} = U_{L,R} \begin{pmatrix} d \\ s \\ b \end{pmatrix}_{L,R}, \tag{2.54}$$

where u, c, t, d, s, b are the quark mass eigenstates, such that

$$U_R^{-1}\mathcal{M}^u U_L = \begin{pmatrix} m_u & 0 & 0 \\ 0 & m_c & 0 \\ 0 & 0 & m_t \end{pmatrix}, \qquad D_R^{-1}\mathcal{M}^d D_L = \begin{pmatrix} m_d & 0 & 0 \\ 0 & m_s & 0 \\ 0 & 0 & m_b \end{pmatrix}. \tag{2.55}$$

Diagonalising the mass matrices $\mathcal{M}^u$ and $\mathcal{M}^d$, simultaneously diagonalises the Yukawa matrices $yYu_{ij} = \sqrt{2}\mathcal{M}^u_{ij}/v$ and $Y^d_{ij} = \sqrt{2}\mathcal{M}^d_{ij}/v$. Rotating the up-type quarks by the matrix U_L, and the down-type quark by matrix D_L, breaks up the left-handed quarks. This shows up in the charged-current weak interactions, which we describe below. This changes $u_{Lj} \leftrightarrow d_{Lj}$ within the same doublets, because the mass eigenstates of the down-type quarks are no longer matched up to the mass eigenstates of the up-type quarks. There is a generation changing weak interation, which are described by the CKM matrix [15].

The quarks have a tendency to mix as we have briefly seen, and we introduced the CKM matrix to describe that, where these can be clearly seen in the charge current interaction.

A CKM matrix, V_{CKM}, is a 3×3 unitary matrix which is responsible for mixing quarks in the SM. This matrix can be parametrised by three mixing angles and the CP-violating phase, which is very small:

$$V_{CKM} \equiv V_L^u V_L^{d\dagger} = \begin{pmatrix} V_{ud} & V_{us} & V_{ub} \\ V_{cd} & V_{cs} & V_{cb} \\ V_{tb} & V_{ts} & V_{tb} \end{pmatrix}. \tag{2.56}$$

This unitary matrix has elements $(V_{CKM})_{ij}$ that can be interpreted as connecting the left handed u-type quarks of the i-th generation with the left handed d-type quarks of the j-th generation.

To describe the charge current interaction between the quarks that are left handed. We shall make use of the kinetic term of the SM. We define the kinetic term as:

$$\mathcal{L}_{kinetic} = i\bar{\psi}(D_\mu \gamma^\mu)\psi, \tag{2.57}$$

with the covariant derivative defined as

$$D_\mu = \partial_\mu + \frac{i}{2} g W_b^\mu \sigma_b + i g' Y B_\mu, \tag{2.58}$$

where σ_b are the Pauli matrices, $b = 1, 2, 3.$ and Y is the hypercharge.

We write

$$\begin{aligned}
\mathcal{L}_{cc} =& i\bar{Q'}_{Li}\gamma^\mu(\partial_\mu + \frac{i}{2} g W_b^\mu \sigma_b) Q'_{Li} \\
=& i(\bar{u\ d})'_{Li}\gamma^\mu(\partial_\mu + \frac{i}{2} g W_b^\mu \sigma_b) \begin{pmatrix} u \\ d \end{pmatrix}'_{Li} \\
=& i\bar{u}'_{Li}\gamma^\mu\partial_\mu u'_{Li} + i\bar{d}'_{Li}\gamma^\mu\partial_\mu d'_{Li} - \frac{g}{\sqrt{2}}\bar{u}'_{Li}\gamma^\mu W^{-\mu} d'_L - \frac{g}{\sqrt{2}}\bar{d}'_{Li}\gamma^\mu W^{+\mu} u'_L,
\end{aligned} \tag{2.59}$$

using $W^\pm = \frac{1}{\sqrt{2}}(W_{1\mu} \mp i W_{2\mu})$ and γ^μ (where $\mu, \nu = 0, 1, 2, 3$) are the Dirac matrices.

To express the Lagrangian in terms of quark mass eigenstates d, u, instead of weak interaction eigenstates, we should observe the quark mixing between generations which appear in the charged current interaction.

$$\begin{aligned}
\mathcal{L} =& \frac{g}{\sqrt{2}}\bar{u}'_{Li}\gamma^\mu W^{-\mu} d'_L + \frac{g}{\sqrt{2}}\bar{d}'_{Li}\gamma^\mu W^{+\mu} u'_L \\
=& \frac{g}{\sqrt{2}}\bar{u}_{Li}(V_L^u V_L^{d\dagger})_{ij}\gamma^\mu W^{-\mu} d_L + \frac{g}{\sqrt{2}}\bar{d}_{Li}(V_L^u V_L^{d\dagger})^*_{ij}\gamma^\mu W^{+\mu} u_L \\
=& \frac{g}{\sqrt{2}}\bar{u}_{Li} V_{CKM}\gamma^\mu W^{-\mu} d_L + \frac{g}{\sqrt{2}}\bar{d}_{Li} V^*_{CKM}\gamma^\mu W^{+\mu} u_L,
\end{aligned} \tag{2.60}$$

with $V_{CKM} = (V_L^u V_L^{d\dagger})_{ij}$.

We choose the interaction eigenstates to be equal to the mass eigenstates for the up-type quarks only, where for the down-type quarks we choose them to be rotated, that is, going from the interaction basis to the mass basis.

We define the mass eigenstates as;

$$u_L = V_{ji} Q'_i, \qquad c_L = V_{ji} Q'_i, \qquad t_L = V_{ji} Q'_i \tag{2.61}$$

$$\bar{u_1} = i\sigma_2 u_R^*, \qquad \bar{u_2} = i\sigma_2 c_R^*, \qquad \bar{u_3} = i\sigma_2 t_R^*. \tag{2.62}$$

In the SM there is CP-violation in the quark sector due to the three generations of quarks, and the charge current interaction. That is, if we apply the CP operator to the charge current interation Lagrangian:

$$\mathcal{L}_{cc} = \frac{g}{\sqrt{2}} \bar{u}_{Li} V_{CKM} \gamma^\mu W^{-\mu} d_L + \frac{g}{\sqrt{2}} \bar{d}_{Li} V^*_{CKM} \gamma^\mu W^{+\mu} u_L \tag{2.63}$$

$$CP(\mathcal{L}_{cc}) = \frac{g}{\sqrt{2}} \bar{d}_{Li} V_{CKM} \gamma^\mu W^{-\mu} u_L + \frac{g}{\sqrt{2}} \bar{u}_{Li} V^*_{CKM} \gamma^\mu W^{+\mu} d_L. \tag{2.64}$$

Applying the CP operator to the Lagrangian, it transforms by changing the two terms and the CKM matrix is conjugated. The CP violation arises because the CKM matrix is complex and $V \neq V^*$.

Finally, note that the neutral currents follow the same path as the charge currents, and are CP-invariant. However, there exists in the SM FCNCs which are absent at tree level, and are induced at one-loop by W boson exchanges, which are typically small effects [16].

2.4 Summary

In this dissertation, we only focused on the scalar sector and the Yukawa sector of the SM, this is because we are interested in the Higgs boson and how it interacts with other particles in the SM. Understanding the SM will serve as important to the next chapter (2HDMs) ss an extension of the SM. Despite the great discussion above, there are inadequacies that allows us to look for other phenomena BSM. To quote the Higgs hunter's guide,"In this book we will repeatedly emphasise that many people who have studied Higgs physics do not expect a single, neutral boson of some definite mass to occur as the only direct manifestation of EWSB" [13]. As a result, theories with several Higgs fields have been studied almost since the beginning of the SM [13]. The most studied case adds an extra scalar doublet to the SM and is called the 2HDM.

Chapter 3

Two Higgs-doublet models

3.1 Motivation

The SM has been a triumphant achievement in particle physics in terms of explaining the laws of nature, it has been regarded as having inadequacies and incomplete because there are phenomena that it doesn't explain. It doesn't include concepts such as the baryonic-asymmetry of the universe [17], the oscillations of neutrinos [18], dark matter candidates [19](which account for most of the matter in the universe), and it doesn't include gravity. This gives us the impetus to investigate more complete theories that will better address these questions, these are what we consider BSM. The 2HDM is a BSM theory which answers some of these questions, such as CP-violation etc. The motivation behind the 2HDM is that when breaking the electroweak symmetry does nature only allow for one scalar field, whereby adding another scalar doublet to the SM we observe some interesting properties, such as the production of additional Higgs particles, sources of CP-violation and FCNCs.

This model has many interesting properties that distinguish it from the SM. The first one is the presence of three neutral scalars and charged scalars, instead of the single Higgs particle that appears in the SM. Recall that the SM, the gauge bosons $(W^{\pm}, Z)$ are massless without the Higgs mechanism, each with only two possible transverse polarisations. With the Higgs mechanism, each has three polarisations (the two transverses and a new longitudinal). This happens as a result of the Higgs doublet, with its four components, two are charged Higgs components and two are neutral. After spontaneously symmetry breaking, the two charged Higgs components and one neutral component are absorbed as the longitudinal components of the $W^{\pm}$ and Z bosons, the fourth component is neutral and corresponds to the Higgs boson.

In 2HDMs everything in the scalar sector is doubled. There are four charged components and four neutral components. Two of them are absorbed by the $W^{\pm}$ bosons and the other charged components are the charged scalar particles $H^{\pm}$. In the neutral components, one is absorbed by the Z boson and the remaining three neutral components corresponds to the neutral particles, of which two of them are the CP-even scalar particle and the third one is the CP-odd scalar particle. This shall now be detailed more explicitly in the next chapter.

3.2 The Scalar sector

The 2HDM scalar sector cosists of two scalar doublets, writting the Lagrangian in it's most general form requires it to be renormalisable and Lorentz invariant.

$$\mathcal{L}_{2HDM} = \mathcal{L}_{\Phi} + \mathcal{L}_{Yukawa} + \mathcal{L}_{SM}^{gauge}; \tag{3.1}$$

the first term is the Lagrangian of the SM with an additional scalar doublet Φ, the second term is the Lagrangian of the positive Yukawa interactions, where this term gives rise to the FCNC (we shall later see how they are suppressed), and the final term is the Lagrangian of the interactions with the SM gauge fields.

Starting with the first term:

$$\mathcal{L}_{\Phi} = (D_{\mu}\Phi_1)^{\dagger}(D^{\mu}\Phi_1) + (D_{\mu}\Phi_2)^{\dagger}(D^{\mu}\Phi_2) - V(\Phi_1\Phi_2), \tag{3.2}$$

where the covariant derivative in standard notation is given by:

$$D_{\mu} = \partial_{\mu} + ig\frac{\tau^i}{2}\cdot W_{\mu}^i + i\frac{g\prime}{2}YB_{\mu}$$

and the potential is:

$$\begin{aligned} V(\Phi_1,\Phi_2) =& m_{11}^2\Phi_1^{\dagger}\Phi_1 + m_{22}^2\Phi_2^{\dagger}\Phi_2 - (m_{12}^2\Phi_1^{\dagger}\Phi_2 + h.c) + \frac{\lambda_1}{2}(\Phi_1^{\dagger}\Phi_1)^2 \\ &+ \frac{\lambda_2}{2}(\Phi_2^{\dagger}\Phi_2)^2 \lambda_3(\Phi_1^{\dagger}\Phi_1)(\Phi_2^{\dagger}\Phi_2) + \lambda_4(\Phi_1^{\dagger}\Phi_2)(\Phi_2^{\dagger}\Phi_1) \\ &+ \left[\frac{\lambda_5}{2}(\Phi_1^{\dagger}\Phi_2)^2 + \lambda_6(\Phi_1^{\dagger}\Phi_1)(\Phi_1^{\dagger}\Phi_2) + \lambda_7(\Phi_2^{\dagger}\Phi_2)(\Phi_1^{\dagger}\Phi_2) + h.c.\right] \text{ [6].} \end{aligned} \tag{3.3}$$

This is the most general potential and is it not CP-invariant as it has both the real and imaginary parameters, where $h.c.$ stands for the hermitian conjugate. The parameters m_{11}^2, m_{22}^2 and $\lambda_{1,2,3,4}$ are real. In general, m_{12}^2 and $\lambda_{5,6,7}$ are complex. Hence

by setting $\lambda_6 = \lambda_7 = 0$, the potential becomes CP-invariant. The CP conservation is imposed at the Lagrangial level, CP can be spontaneously broken provided that no other discrete symmetry is imposed on the Lagrangian. This is refered as Lee's model [20]

The scalar sector of the 2HDM has many interesting features, in its most general form the potential apparently has 14 independent parameters. The scalar potential determines the vacuum of the 2HDM, and this vacuum is not unique. This basic requirement that the potential should be bounded from below ensures that the minimum is stable, and this imposes constraints on the quartic couplings.

To discuss the stabiliy of the potential it is convenient to work with Eqn. (3.3). In order for it to be bounded from below, the quartic terms in Eqn. (3.3) should not tend to minus infinity in any direction in the parameter space and be positive. The potential with the above choice of $\lambda_6 = \lambda_7 = 0$, and when we choose a direction of the scalar field, such that $|\Phi_1| \to \infty$ and $|\Phi_2| = 0$. Then along this direction the quartic terms are bounded from below and go to infinity as $\lambda_1/2|\Phi|^2$. If we want this limit to be positive or zero we need $\lambda_1 \gg 0$. Also by choosing $|\Phi_2| \to \infty$ and $|\Phi_1| = 0$, we can obtain $\lambda_2 \gg 0$. If we take the direction $|\Phi_1|^2 = r\cos\theta$, $|\Phi_1|^2 = r\sin\theta$ and $\Phi_1^\dagger \Phi_2 = 0$, the potential shall always be greater or equal to zero at infinity along the direction

$$\frac{\lambda_1}{2}\cos^2\theta + \frac{\lambda_2}{2}\sin^2\theta + \lambda_3 \sin\theta\cos\theta \geqslant 0 \text{ [6]}, \tag{3.4}$$

for $0 \leqslant \theta \leqslant \pi/2$. The potential is bounded below if and only if the following conditions are obeyed:

$$\begin{aligned} &\lambda_1 \geqslant 0, \qquad \lambda_2 \geqslant 0 \\ &\lambda_3 \geqslant -\sqrt{\lambda_1\lambda_2}, \qquad \lambda_3 + \lambda_4 - |\lambda_5| \geqslant -\sqrt{\lambda_1\lambda_2} \text{ [6]}. \end{aligned} \tag{3.5}$$

The most general form of the vev up to a gauge transformation is:

$$\langle 0|\Phi_1|0\rangle = \begin{pmatrix} 0 \\ \frac{v_1}{\sqrt{2}} \end{pmatrix}, \qquad \langle 0|\Phi_2|0\rangle = \begin{pmatrix} v' \\ \frac{v_2}{\sqrt{2}} \end{pmatrix} e^{i\theta}, \tag{3.6}$$

where $v_1, v_2, v' \geqslant 0$. While in the SM the electric charge and CP are not spontaneously broken by the Higgs vev, the situation changes in the 2HDM, where depending on the form of the potential and value of the parameters, charge violating minima and CP violating minima can arise. In fact, the electric charge is broken if

$v' \neq 0$ and CP is broken if $e^{i\theta} \neq \pm 1$. Accordingly, three different types of vacua can be defined for a general 2HDM with all constants real, Φ_1 is a vacuum expectation value for the first doublet scalar field and Φ_2 is expectation value of the second doublet scalar field:

$$\langle 0|\Phi_1|0\rangle_N = \begin{pmatrix} 0 \\ \frac{v_1}{\sqrt{2}} \end{pmatrix}, \qquad \langle 0|\Phi_2|0\rangle_N = \begin{pmatrix} 0 \\ \frac{v_2}{\sqrt{2}} \end{pmatrix}, \tag{3.7}$$

which is the normal vacuum;

$$\langle 0|\Phi_1|0\rangle_{CB} = \begin{pmatrix} 0 \\ \frac{v_1'}{\sqrt{2}} \end{pmatrix}, \qquad \langle 0|\Phi_2|0\rangle_{CB} = \begin{pmatrix} \frac{\alpha}{\sqrt{2}} \\ \frac{v_2'}{\sqrt{2}} \end{pmatrix}, \tag{3.8}$$

for a vacuum that breaks charge conservation, that is, the vev $\alpha/\sqrt{2} \neq 0$ breaks charge conversation and would give mass to the photon; finally

$$\langle 0|\Phi_1|0\rangle_{CP} = \begin{pmatrix} 0 \\ \frac{\bar{v_1}}{\sqrt{2}} \end{pmatrix}, \qquad \langle 0|\Phi_2|0\rangle_{CP} = \begin{pmatrix} 0 \\ \frac{\bar{v_2}}{\sqrt{2}} \end{pmatrix} e^{i\theta}, \tag{3.9}$$

for a CP breaking vacuum. From now on we shall assume the minimisation of the Higgs potential leads to a normal vacuum. The 2HDM consists of a rich spectrum of vevs, such as the neutral minima, the charge breaking minima and CP breaking minima [6]. The most general complex scalars in 2HDMs have the following form, which introduces eight fields Φ_i, ρ_i and $\eta_i (i = 1, 2)$:

$$\Phi_a = \begin{pmatrix} \Phi_a^+ \\ \frac{1}{\sqrt{2}}(v_a + \rho_a + i\eta_a) \end{pmatrix}, \qquad a = 1, 2.$$

Expanding the doublet around the the minima and inserting the fields into the potential generates terms that are linear in the fields:

$$\left.\frac{\partial V}{\partial \Phi_1^+}\right|_{\langle\phi_1\rangle,\langle\phi_2\rangle} = 0, \qquad \left.\frac{\partial V}{\partial \Phi_2^+}\right|_{\langle\phi_1\rangle,\langle\phi_2\rangle} = 0. \tag{3.10}$$

Computing Eqn.(3.3) we get the following results, which are the mass-squared matrices:

$$m_{11}^2 = m_{12}^2 \frac{v_2}{v_1} - \frac{\lambda_1}{2} v_1^2 - (\lambda_1 + \lambda_4 + \lambda_5)\frac{v_2^2}{2}, \tag{3.11}$$

$$m_{22}^2 = m_{12}^2 \frac{v_1}{v_2} - \frac{\lambda_1}{2} v_1^2 - (\lambda_1 + \lambda_4 + \lambda_5)\frac{v_1^2}{2}. \tag{3.12}$$

The expansion of these scalar doublets in the 2HDM potential generates terms that are bilinear in the fields $\Phi_i^\pm, \rho_i$ and η_i. Since these bilinear terms contribute to the

propagators of the eight fields, they give rise to the mass terms. All bilinear terms in the 2HDM potential can be brought into the form:

$$V = \frac{1}{2}\big(\rho_1, \rho_2\big)\mathcal{M}_\rho{}^2 \begin{pmatrix} \rho_1 \\ \rho_2 \end{pmatrix} + \frac{1}{2}\big(\eta_1, \eta_2\big)\mathcal{M}_\eta{}^2 \begin{pmatrix} \eta_1 \\ \eta_2 \end{pmatrix} + \frac{1}{2}\big(\phi_1^+, \phi_2^+\big)\mathcal{M}_{\phi^\pm}{}^2 \begin{pmatrix} \phi_1^- \\ \phi_2^- \end{pmatrix}. \tag{3.13}$$

The explicit form of the non-diagonal mass matrices of the CP-even scalars, CP-odd scalar and the charged Higgs boson can be written as follows after the expansion:

$$\mathcal{M}_\rho{}^2 = -\frac{1}{2}(\rho_1, \rho_2) \begin{pmatrix} m_{12}^2 \frac{v_2}{v_1} + \lambda_1 v_1^2 - & m_{12}^2 + \lambda_{345} v_1 v_2 \\ -m_{12}^2 + \lambda_{345} v_1 v_2 & m_{12}^2 \frac{v_2}{v_1} + \lambda_1 v_2^2 \end{pmatrix} \begin{pmatrix} \rho_1 \\ \rho_2 \end{pmatrix}, \tag{3.14}$$

$$\mathcal{M}_\eta{}^2 = -\frac{1}{2}\frac{m_A^2}{v_1^2 + v_2^2}(\eta_1, \eta_2) \begin{pmatrix} v_2^2 & -v_1 v_2 \\ -v_1 v_2 & v_1^2 \end{pmatrix} \begin{pmatrix} \eta_1 \\ \eta_2 \end{pmatrix}, \tag{3.15}$$

$$\mathcal{M}_{\phi^\pm}{}^2 = -[m_{12}^2 - (\lambda_4 + \lambda_5)\frac{v_1 v_2}{2}](\phi_1^-, \phi_2^-) \begin{pmatrix} \frac{v_2}{v_1} & -1 \\ -1 & \frac{v_1}{v_2} \end{pmatrix} \begin{pmatrix} \phi_1^+ \\ \phi_2^+ \end{pmatrix}. \tag{3.16}$$

The eigenstates masses can be achieved by diagonalising the matrices above. This means that the $\mathcal{M}_\rho{}^2, \mathcal{M}_\eta{}^2$ and $\mathcal{M}_{\phi^\pm}{}^2$ matrices have some R_α and R_β such that,

$$D_\rho^2 = R_\alpha^T \mathcal{M}_\rho{}^2 R_\alpha, \tag{3.17}$$

$$D_\eta^2 = R_\beta^T \mathcal{M}_\eta{}^2 R_\beta, \tag{3.18}$$

$$D_{\phi^\pm}^2 = R_\alpha^T \mathcal{M}_{\phi^\pm}{}^2 R_\alpha. \tag{3.19}$$

These R_α and R_β are diagonal matrices. The spectral theorem states that for real-valued, symmetric matrices, the transformation matrices R_α and R_β are orthogonal. The matrices can be paramertrised by two angles α and β, and defined with the explicit form:

$$R_\alpha = \begin{pmatrix} \cos\alpha & -\sin\alpha \\ \sin\alpha & \cos\alpha \end{pmatrix}, \qquad R_\beta = \begin{pmatrix} \cos\alpha & -\sin\alpha \\ \sin\alpha & \cos\alpha \end{pmatrix}. \tag{3.20}$$

Because we have assumed CP-invariance, the imaginary part and the real part of the neutral scalar decouples and we shall write the imaginary part as the CP-odd scalar (A^0). This shall lead us to have a neutral Goldstone boson (G^0) and the real part are the CP-even scalars (H^0, h^0), which are the combination of the bilinear terms after applying the diagonalisation procedure to the 2HDM potential. The mass matrix of the charged scalars has a zero eigenvalue which corresponds to the

charged Goldstone boson ($G^{\pm}$):

$$V = \frac{1}{2}\Big(H^0, h^0\Big) {D_\rho}^2 \begin{pmatrix} H^0 \\ h^0 \end{pmatrix} + \frac{1}{2}\Big(G^0, A^0\Big) {D_\eta}^2 \begin{pmatrix} G^0 \\ A^0 \end{pmatrix} + \frac{1}{2}\Big(G^+, H^+\Big) {D_{\phi^\pm}}^2 \begin{pmatrix} G^- \\ H^- \end{pmatrix}. \tag{3.21}$$

The fields $\phi_i^\pm, \rho_i, \eta_i$ in the gauge basis are transformed into physical fields:

$$\begin{pmatrix} H^0 \\ h^0 \end{pmatrix} = \begin{pmatrix} c_\alpha & s_\alpha \\ -s_\alpha & c_\alpha \end{pmatrix} \begin{pmatrix} \rho_1 \\ \rho_2 \end{pmatrix}, \tag{3.22}$$

$$\begin{pmatrix} G^0 \\ A^0 \end{pmatrix} = \begin{pmatrix} c_\beta & s_\beta \\ -s_\beta & c_\beta \end{pmatrix} \begin{pmatrix} \eta_1 \\ \eta_2 \end{pmatrix}, \tag{3.23}$$

$$\begin{pmatrix} G^\pm \\ H^\pm \end{pmatrix} = \begin{pmatrix} c_\beta & s_\beta \\ -s_\beta & c_\beta \end{pmatrix} \begin{pmatrix} \phi_1^\pm \\ \phi_2^\pm \end{pmatrix}. \tag{3.24}$$

The CP-even scalars with the parameter α, which mixes the states:

$$H^0 = -\rho_1 \cos\alpha - \rho_2 \sin\alpha, \tag{3.25}$$

$$h^0 = \rho_1 \sin\alpha - \rho_2 \cos\alpha. \tag{3.26}$$

The neutral Goldstone boson is orthogonal to the CP-odd scalar and the η_j is a linear combination to the CP-odd scalar:

$$G^0 = \eta_1 \cos\beta + \eta_2 \sin\beta, \tag{3.27}$$

$$A^0 = \eta_1 \sin\beta - \eta_2 \cos\beta. \tag{3.28}$$

The mass matrices are diagonal and the entries of the mass matrices are masses of the physical fields:

$$D_\rho^2 = \begin{pmatrix} m_{H^0}^2 & 0 \\ 0 & m_{h^0}^2 \end{pmatrix}, \tag{3.29}$$

$$D_\eta^2 = \begin{pmatrix} m_{G^0}^2 & 0 \\ 0 & m_{A^0}^2 \end{pmatrix}, \tag{3.30}$$

$$D_{\phi^\pm}^2 = \begin{pmatrix} m_{G^\pm}^2 & 0 \\ 0 & m_{H^\pm}^2 \end{pmatrix}. \tag{3.31}$$

Thus the tree-level masses of the the particles in the mass basis are as follows:

$$m^2_{H^0,h^0} = \frac{1}{2}\left[\mathcal{M}^2_{11} + \mathcal{M}^2_{12} \pm \sqrt{(\mathcal{M}^2_{11} - \mathcal{M}^2_{22})^2 + 4(\mathcal{M}^2_{12})^2}\right], \tag{3.32}$$

$$m^2_{A^0} = v^2\left(\frac{m^2_{12}}{v_1 v_2} - \lambda_5\right), \qquad m^2_{G^0} = 0, \tag{3.33}$$

$$m^2_{H^\pm} = v^2\left(\frac{m^2_{12}}{v_1 v_2} - \frac{\lambda_4 + \lambda_5}{2}\right), \qquad m^2_{G^\pm} = 0. \tag{3.34}$$

The mixing angle α is given in terms of

$$\sin 2\alpha = \frac{2\mathcal{M}_{12}}{\sqrt{(\mathcal{M}_{12} - \mathcal{M}_{22})^2 + 4\mathcal{M}^2_{12}}}, \tag{3.35}$$

and

$$\cos 2\alpha = \frac{\mathcal{M}_{11} - \mathcal{M}_{22}}{\sqrt{(\mathcal{M}_{12} - \mathcal{M}_{22})^2 + 4\mathcal{M}^2_{12}}}. \tag{3.36}$$

The massless particles G^0 and $G^\pm$ are the three Goldstone bosons of the 2HDM, and are absorbed to give mass to the $W^\pm, Z^0$ gauge bosons. The remaining five physical particles are H^0 (heavy) and h^0 (lighter), which are the CP-even particles, A^0 is the CP-odd, and the two particles $H^\pm$ are the charged Higgs bosons.

In the 2HDM we also have the alignment of states [21]. This allows us to make the observed lighter Higgs boson to be the SM-like boson, and the other neutral Higgs boson to be a heavy Higgs boson. When the alignment limit is attained in the decoupling limit the additional Higgs bosons are made very heavy. The alignment limit is the limit in which one of the two neutral CP-even Higgs mass eigenstates aligns with the direction of the scalar field vacuum expectation values. The alignment limit is independent of the choice of basis for the two Higgs doublet fields. The alignment limit makes the couplings of the gauge boson to the Higgs boson approach those of towards the SM value. The corresponding coupling VV, where $V = W^\pm, Z$, to the Higgs boson is denoted by C^ϕ_V ($\phi = h, H$), it follows that;

$$C^h_V = \sin(\beta - \alpha), \qquad C^H_V = \cos(\beta - \alpha). \tag{3.37}$$

The couplings of the CP-even Higgs scalars, CP-odd Higgs scalars and the charged Higgs scalars to fermions are shown in the next section.The alignment limit corresponds either to the limit of $\cos(\beta - \alpha) \to 0$ if h is identified as the SM-like Higgs boson or to the limit of $\sin(\beta - \alpha) \to 0$ if H is identified as the SM-like Higgs boson.

The physical mass eigenstates are then defined as follows:

$$H = (\sqrt{2}ReH_1^0 - v)\cos(\beta - \alpha) - \sqrt{2}ReH_2^0 \sin(\beta - \alpha), \tag{3.38}$$

$$h = (\sqrt{2}ReH_1^0 - v)\sin(\beta - \alpha) - \sqrt{2}ReH_2^0 \cos(\beta - \alpha). \tag{3.39}$$

The neutral CP-even Higgs scalar mass eigenstates is approximately aligned in the direction of the vev, this is called the alignment limit [22]. In the next section we shall study the Yukawa interactions of the 2HDMs Higgs bosons, and their branching ratios

3.3 The Yukawa interaction

Yukawa interactions are a coupling of a scalar field Φ with a fermionic field of the form $Y\bar{\psi}\Phi\psi$, where Y is a coupling constant. If the scalar field Φ is Higgs doublet, then through spontaneous symmetry breaking the fermions acquire mass. This is how mass is introduced in the SM, and it is proportional to the Higgs field's vev. Writing out the Yukawa terms for a 2HDM

$$\begin{aligned} -\mathcal{L}_{Yukawa} =& Y_{ij}^{l1}\bar{e}_{Ri}\Phi_1^\dagger L_{Lj} + Y_{ij}^{d1}\bar{d}_{Ri}\Phi_1^\dagger Q_{Lj} + Y_{ij}^{u1}\bar{u}_{Ri}\Phi_1^\dagger Q_{Lj} \\ &+ Y_{ij}^{l2}\bar{e}_{Ri}\Phi_2^\dagger L_{Lj} + Y_{ij}^{d2}\bar{d}_{Ri}\Phi_2^\dagger Q_{Lj} + Y_{ij}^{u2}\bar{u}_{Ri}\Phi_2^\dagger Q_{Lj} + h.c..[6] \end{aligned} \tag{3.40}$$

the Y's are complex 3×3 matrices of Yukawa couplings and $i, j = 1, 2, 3$ are the generation indices. This Lagrangian gives us some trouble when we want to diagonalise the mass-matrices. By this we mean that if we focus on the down-type quark mass term:

$$\mathcal{L}_{Yukawa} = -(Y_{ij}^{d1}\Phi_1^\dagger + Y_{ij}^{d2}\Phi_2^\dagger)\bar{d}_{Ri}Q_{Lj} + h.c., \tag{3.41}$$

and by considering the vev's of the scalar fields, we plug them in to define the mass-matrix in the following way;

$$\mathcal{M}_{ij}^d = \left(Y_{ij}^{d1}\frac{v_1}{\sqrt{2}} + Y_{ij}^{d2}\frac{v_2}{\sqrt{2}}\right). \tag{3.42}$$

Applying the same procedure as in chapter 2, we can diagonalise this mass matrix, which means that we can diagonalise the linear combination of Y^{d1} and Y^{d2}, which are the coefficients of the down-type quark. The problem arises when we can't diagonalise the orthogonal linear combination of Y^{d1} and Y^{d2}, hence we say that it

is impossible to diagonalise the Yukawa coupling matrices simultaneously, and this can in general, cases can to FCNCs. More detailed examples have been shown for the $A^0\bar{s}d$ vertex and $K^0 - \bar{K^0}$ mixing in Ref. [23]. We can say the same thing about the up-type quarks.

These processes would in general lead to experimental inconsistencies, and we should try to avoid them in most cases. Various solutions to these processes have been suggested, and the one we shall discuss is by introducing a discrete set of symmetries known as Z_2 symmetries, as proposed by the Glashow-Weinberg-Paschos theorem [24]. This theorem states that a necessary and sufficient condition for the absence of FCNCs at tree level is that all fermions of a given charge and helicity transform according to the same irreducible representation of $SU(2)$, corresponding to the eigenvalue of T_3, and that a basis exists in which they receive their contributions in the mass matrix from a single source. The philosophy of this approach is to split the 2HDM into types, where one of the doublets couples to the up-quark type, and the other doublet couples to the down-quark, as in table 3.1

When we insert the vev of the scalar fields and impose a Z_2 symmetry on the 2HDM, it splits into four different types. These symmetries are defined as $\Phi_1 \to -\Phi_2, \Phi_1 \to \Phi_2$, and it suppresses FCNCs in the Yukawa interactions. The four types are:

- Type I - Only Φ_2 couples to fermions and gives mass to all particles (quarks and leptons),
- Type II - Φ_1 couples to the down-type quarks and leptons, while Φ_2 couples only to the up-type quarks and neutrinos,
- Type X (lepton specific) - Φ_2 couples to the up-type and down-type quarks, and Φ_1 couples to the leptons only,
- Type Y (Flipped) - Φ_2 couples to the up-type quarks and leptons, and Φ_1 couples to the down-type.

When we insert the vev of Φ_2 into the scalar doublet for a Type I 2HDM, then it gives mass to the fermions as:

$$\begin{aligned} -\mathcal{L}_I &= Y_{ij}^{l2}\bar{e}_{Ri}\Phi_2^\dagger L_{Lj} + Y_{ij}^{d2}\bar{d}_{Ri}\Phi_2^\dagger Q_{Lj} + Y_{ij}^{u2}\bar{u}_{Ri}\tilde{\Phi_2}^\dagger Q_{Lj} + h.c. \\ &= Y_{ij}^{l2}\bar{e}_{Ri}\frac{v_2}{\sqrt{2}}e_{Lj} + Y_{ij}^{d2}\bar{d}_{Ri}\frac{v_2}{\sqrt{2}}d_{Lj} + Y_{ij}^{u2}\bar{u}_{Ri}\frac{v_2}{\sqrt{2}}u_{Lj} + h.c. \\ &= \frac{Y_{ij}^{l2}}{\sqrt{2}}v_2\bar{e}_{Ri}e_{Lj} + \frac{Y_{ij}^{d2}}{\sqrt{2}}v_2\bar{d}_{Ri}d_{Lj} + \frac{Y_{ij}^{u2}}{\sqrt{2}}v_2\bar{u}_{Ri}u_{Lj} + h.c.. \end{aligned} \tag{3.43}$$

The masses of the fermions can be explicitly identified as

$$m_{l,d,u} = \frac{Y_2^{l2,d2,u2}}{\sqrt{2}} v \sin\beta. \tag{3.44}$$

Note that in type-I and type-II, the right handed leptons satisfy the discrete symmetry as the d_R^i and thus the leptons couple to the same Higgs boson as $Q = -1/3$ quarks. In the leptonic-specific type, the right handed quarks all couple to Φ_2 and the right handed leptons couple to Φ_1. In the flipped type, one has $Q = 2/3$ right handed quarks coupling to Φ_2 and the $Q = -1/3$ right handed quarks coupling to Φ_1, as in the type-II, but now the right handed leptons couple to Φ_2.

When we insert the vev of Φ_1 and Φ_2 in the scalar doublets for a Type II 2HDM, then it gives mass to the fermions as:

$$\begin{aligned} -\mathcal{L}_I &= Y_{ij}^{l1} \bar{e}_{Ri} \Phi_1^\dagger L_{Lj} + Y_{ij}^{d1} \bar{d}_{Ri} \Phi_1^\dagger Q_{Lj} + Y_{ij}^{u2} \bar{u}_{Ri} \tilde{\Phi_2}^\dagger Q_{Lj} + h.c. \\ &= Y_{ij}^{l1} \bar{e}_{Ri} \frac{v_1}{\sqrt{2}} e_{Lj} + Y_{ij}^{d1} \bar{d}_{Ri} \frac{v_1}{\sqrt{2}} d_{Lj} + Y_{ij}^{u2} \bar{u}_{Ri} \frac{v_2}{\sqrt{2}} u_{Lj} + h.c. \\ &= \frac{Y_{ij}^{l1}}{\sqrt{2}} v_1 \bar{e}_{Ri} e_{Lj} + \frac{Y_{ij}^{d1}}{\sqrt{2}} v_1 \bar{d}_{Ri} d_{Lj} + \frac{Y_{ij}^{u2}}{\sqrt{2}} v_2 \bar{u}_{Ri} u_{Lj} + h.c.. \end{aligned} \tag{3.45}$$

The masses of the fermions can be explicitly identified as

$$m_u = \frac{Y_2^{u2}}{\sqrt{2}} v \sin\beta \qquad m_{d,l} = \frac{Y_1^{d1,l1}}{\sqrt{2}} v \cos\beta. \tag{3.46}$$

Using the fact that $v_2 = v \sin\beta$ and $v_1 = v \cos\beta$, rearranging Eqn.(3.16), we get the appropriate Yukawa mass matrix as:

$$Y_f = \frac{\sqrt{2} m_f}{v \sin\beta}, \tag{3.47}$$

where β is defined as $\tan\beta = v_2/v_1$. We also consider α as the mixing angle of CP-even scalars, we require that the Y_f be small, such that when we perform a pertubative expansion and the coupling becomes consistent. The coupling for the $h^0 f\bar{f}$ and $H^0 f\bar{f}$ takes form:

$$\begin{aligned} h^0 f\bar{f} &: -i \frac{m_f}{v} \frac{\cos\alpha}{\sin\beta}, \\ H^0 f\bar{f} &: -i \frac{m_f}{v} \frac{\sin\alpha}{\sin\beta}. \end{aligned}$$

Table 3.1: *Models which lead to natural flavour conservation. The superscript i is a generation index.*

Models	Type I	Type II	(Leptonic-specific)	(Flipped)
u_R^i	Φ_2	Φ_2	Φ_2	Φ_2
d_R^i	Φ_2	Φ_1	Φ_2	Φ_1
e_R^i	Φ_2	Φ_2	Φ_1	Φ_2

Table 3.2: *Yukawa couplings of u, d, l to the neutral Higgs bosons h^o, H^0, A in the four different types.*

Models	Type I	Type II	(Leptonic-specific)	(Flipped)
ζ_h^u	$\cos\alpha/\sin\beta$	$\cos\alpha/\sin\beta$	$\cos\alpha/\sin\beta$	$\cos\alpha/\sin\beta$
ζ_h^d	$\cos\alpha/\sin\beta$	$-\sin\alpha/\cos\beta$	$\cos\alpha/\sin\beta$	$-\sin\alpha/\cos\beta$
ζ_h^l	$\cos\alpha/\sin\beta$	$-\sin\alpha/\cos\beta$	$-\sin\alpha/\cos\beta$	$\cos\alpha/\sin\beta$
ζ_H^u	$\sin\alpha/\sin\beta$	$\sin\alpha/\cos\beta$	$\sin\alpha/\cos\beta$	$\sin\alpha/\cos\beta$
ζ_H^d	$\sin\alpha/\sin\beta$	$\cos\alpha/\sin\beta$	$\sin\alpha/\cos\beta$	$\cos\alpha/\sin\beta$
ζ_H^l	$\sin\alpha/\sin\beta$	$\cos\alpha/\sin\beta$	$\cos\alpha/\sin\beta$	$\sin\alpha/\cos\beta$
ζ_A^u	$\cot\beta$	$\cot\beta$	$\cot\beta$	$\cot\beta$
ζ_A^d	$-\cot\beta$	$\tan\beta$	$-\cot\beta$	$\tan\beta$
ζ_A^l	$-\cot\beta$	$\tan\beta$	$\tan\beta$	$-\cot\beta$

We have used the following relationship between the left and right handed fields

$$\begin{aligned}\bar{\psi}\psi &= (\bar{\psi}^L + \bar{\psi}^R)(\psi^L + \psi^R) \\ &= \frac{1}{2}\Big[\bar{\psi}^L(1+\gamma^5) + \bar{\psi}^R(1-\gamma^5)\Big]\frac{1}{2}\Big[(1-\gamma^5)\psi^L + (1+\gamma^5)\psi^R\Big] \\ &= \bar{\psi}^L\psi^R + \bar{\psi}^R\psi^L.\end{aligned} \tag{3.48}$$

We notice that the coupling is the same as in the SM:

$$\begin{aligned}\mathcal{L}_{Yukawa} = &-\sum_{f=u,d,l}\frac{m_f}{v}(\zeta_h^f\bar{f}fh + \zeta_H^f\bar{f}fH - i\zeta_h^A\bar{f}\gamma^5 fA) \\ &-\frac{\sqrt{2}V_{ud}}{v}\bar{u}(m_u\zeta_A^u P_L + m_d\zeta_A^d P_R)dH^+ + \frac{\sqrt{2}m_l\zeta_A^l}{v}\bar{\nu}_L l_R H^+ + h.c.,\end{aligned} \tag{3.49}$$

where h, H, A and H^+ are the SM-like Higgs, scalar CP-even neutral Higgs, CP-odd neutral Higgs and the charged Higgs fields. The u, d and l are up-type quark, down-type quark and lepton fields. $P_{L/R}$ are the projection operators for the left-handed or right-handed fermions, and the factors ζ are shown in table 3.2 for different types where the factors are expressed in terms of trigonometric functions of the parameters α and β.

3.3.1 Branching of the scalars in 2HDM

In this sub-section, we discuss the difference in decays of the Higgs bosons for the types of Yukawa interactions in the 2HDM. In this case, $H, A, H^{\pm}$ mainly decays into fermions pairs. The decay patterns are therefore completely different among the different types of Yukawa interactions. We only plotted the branching ratios against $\tan\beta$, as $\tan\beta$ is a physical parameter of the model, We have verified the results as in Ref. [25] using the `HDecay-5.10` [26] package, where we also show the explicit calculation in Appendix A .

In Fig. 3.1, we show the branching ratios of H for $m_H = 150$ GeV, $\sin(\beta-\alpha) = 1$ for all types of Yukawa interactions. In type-I, the decay of H into gauge boson $\gamma\gamma$ are not always suppressed and shows to increase for large $\tan\beta$ values. However, the fermionic decays are suppressed in all types of Yukawa interactions.

In Fig. 3.2, we again show the branching ratios of the A for $m_A = 150$ GeV, $\sin(\beta-\alpha) = 1$ for all types of Yukawa interactions. In these results there is no such an enhancement of the bosonic decay modes, it cannot be seen because there is no AH^+H^- coupling.

In Fig. 3.4, is the branching ratios of $H^{\pm}$ for $m_{H^{\pm}} = 150$ GeV, $\sin(\beta-\alpha) = 1$ for all types of Yukawa interactions. The dominant decay is $H^{\pm} \to \tau\nu$ for $\tan\beta > 1$

The CP-even (H) and CP-odd (A) scalars are mass degenerate and their branching ratios are strongly dependant on $\tan\beta$. The CP-even and CP-odd scalars mostly decay into fermions and also to vector bosons. The reason for this is that the couplings between the CP-odd and the vector bosons vanishes and the coupling between the CP-even and vector boson are very small.

For large $\tan\beta$, the Higgs phenomenology is different from that of the SM Higgs boson, and the $b\bar{b}$ and $\tau^+\tau^-$ channels occurs, and these final states dominate in the decay modes when $\tan\beta$ is large in all Types. The decay of CP-even Higgs boson into the gauge boson pair $\gamma\gamma$ and $Z\gamma$ increases for large $\tan\beta$, because all fermionic decays are suppressed.

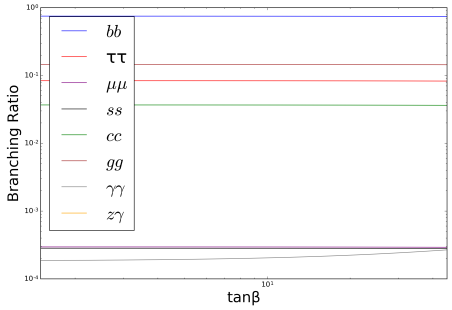

(a) *Branching ratio vs* $\tan\beta$ *for Type I 2HDM*

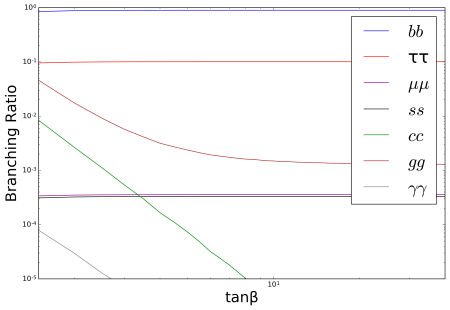

(b) *Branching ratio vs* $\tan\beta$ *for Type II 2HDM*

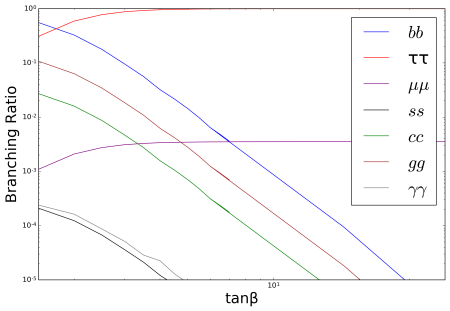

(c) *Branching ratio vs* $\tan\beta$ *for Type X (lepton specific) 2HDM*

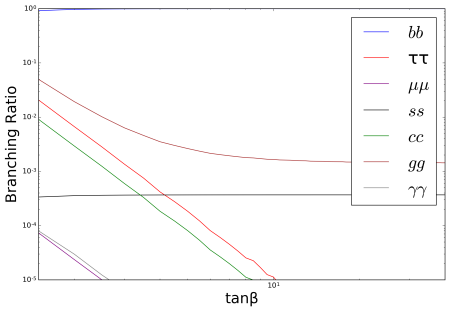

(d) *Branching ratio vs* $\tan\beta$ *for Type Y (Flipped) 2HDM*

Figure 3.1: *Branching ratios of* H *in four different types of 2HDM as function of* $\tan\beta$ *for* $m_H = 150$ *GeV with* $\sin(\beta - \alpha) = 1$.

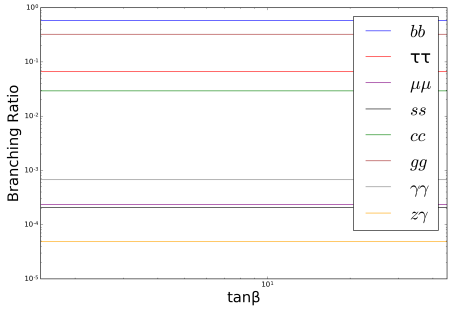

(a) *Branching ratio vs* $\tan\beta$ *for Type X 2HDM*

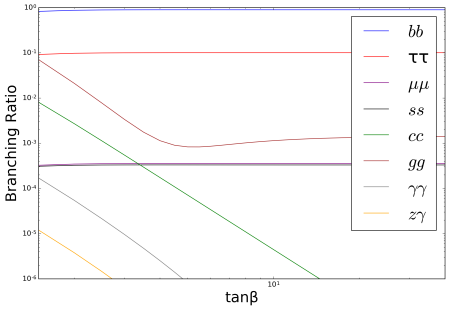

(b) *Branching ratio vs* $\tan\beta$ *for Type X 2HDM*

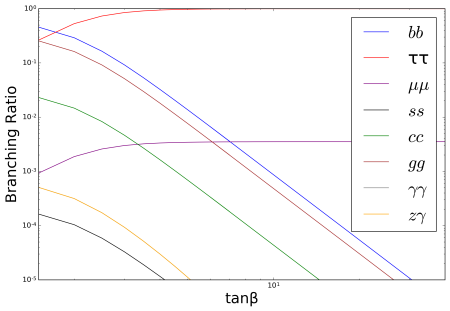

(c) *Branching ratio vs* $\tan\beta$ *for Type Y 2HDM*

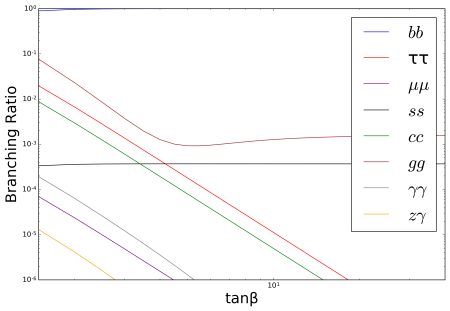

(d) *Branching ratio vs* $\tan\beta$ *for Type Y 2HDM*

Figure 3.2: *Branching ratios of A in four different types of 2HDM as function of* $\tan\beta$ *for* $m_H = 150$ *GeV with* $\sin(\beta - \alpha) = 1$.

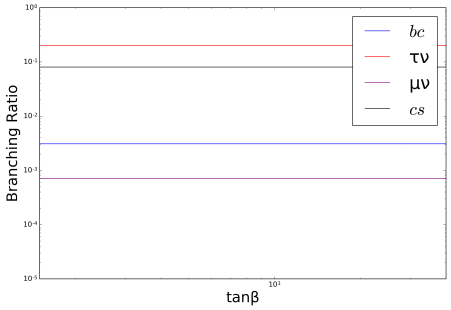

(a) *Branching ratio vs* $\tan\beta$ *for Type I 2HDM*

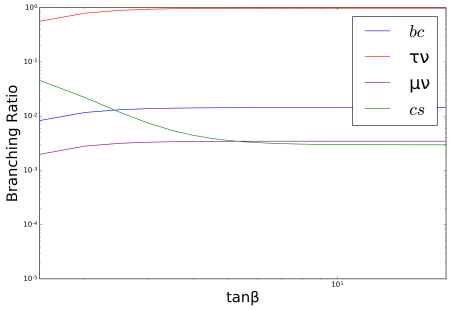

(b) *Branching ratio vs* $\tan\beta$ *for Type 2 2HDM*

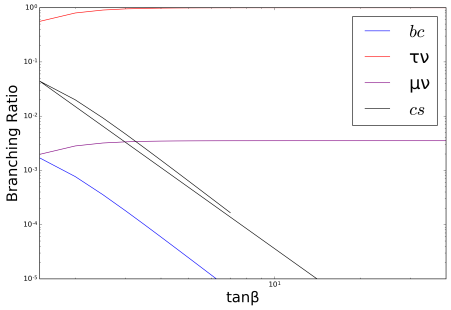

(c) *Branching ratio vs* $\tan\beta$ *for Type X 2HDM*

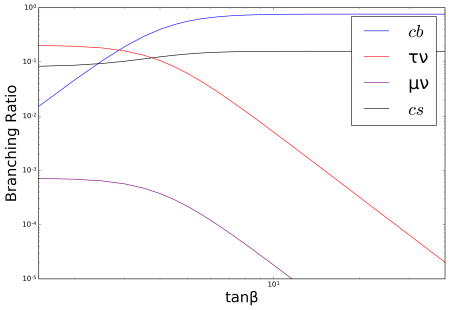

(d) *Branching ratio vs* $\tan\beta$ *for Type Y 2HDM*

Figure 3.3: *branching ratios of* H, A *and* $H^{\pm}$ *in four the different types of 2HDMs as a function of* $\tan\beta$ *for* $m_H = m_A = m_{H^{\pm}} = 150$ *GeV. We have taken the alignment limit* $\sin(\beta - \alpha) = 1$.

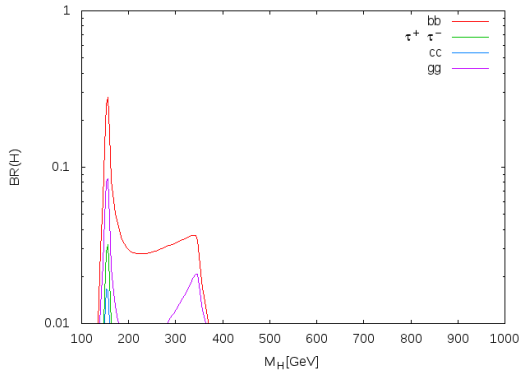

(a) *Branching ratio vs* m_H

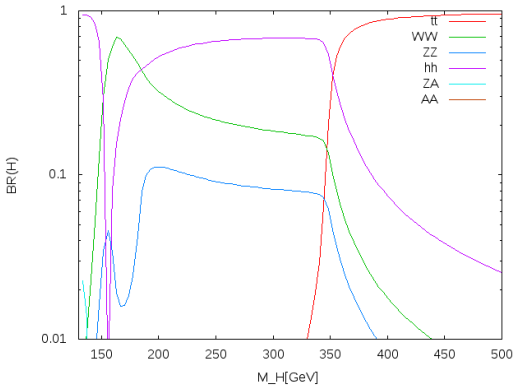

(b) *Branching ratio vs* m_H

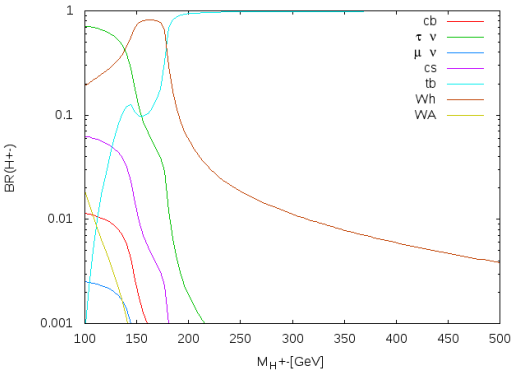

(c) *Branching ratio vs* $m_{H^\pm}$

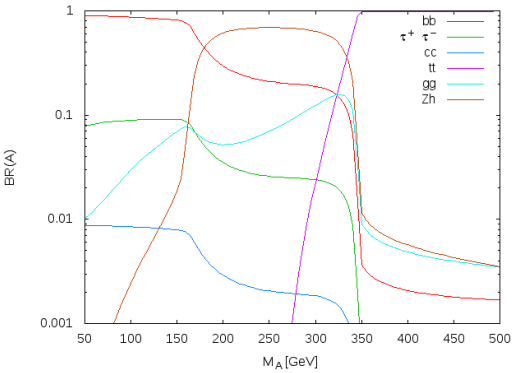

(d) *Branching ratio vs* m_A

Figure 3.4: *Branching ratio vs* m_ϕ*, where* $\phi = m_H = m_A = m_{H^\pm}$ *with* $\tan\beta = 1$.

The plots in Fig. 3.4 describe the relationship between the branching ratio and the masses of the 2HDM, this results are for Type II 2HDM. In the case for the heavy Higgs we see that when the mass of the heavy Higgs is $m_H > 200$ GeV the dominant channel is $H \to hh$, as we shall discussin the next section of the Madala hypothesis, hh is presumed to be dominant channel as is the presumption of the Madala hypothesis.

3.4 The Madala Hypothesis

The Madala hypothesis is a particular BSM as it introduces new physics (NP) in the form of additional scalars. Two of these scalars are heavy scalars, where one is a dark matter (DM) candidate (χ) which is assumed to be a scalar, the other is called the Madala boson (H). Madala is the Zulu word for old and wise man, the connotation being that the Madala boson is older and therefore heavier, than the Higgs boson.

The Madala hypothesis uses H and χ to predict a distorted Higgs boson transverve momentum (p_T) spectrum through the effective decay $H \to h\chi\chi$ [27]. H could be associated with the Type-II 2HDM as a heavy CP-even scalar. The DM candidate is present in the 2HDM only in the inert models. The Madala boson was considered to have Higgs-like couplings to the SM particles, as well as being a source of resonant di-Higgs production. It was therefore considered to have a mass range of $2m_h < m_H < 2m_t$ [28]. Our choice of parameters for this dissertation will draw on the Madala hypothesis by making the heavy scalar mass $m_H = 270$ GeV.

Producing the SM Higgs (h) required consideration the ggh and $\gamma\gamma h$ effective vertices. This can be shown by calculating the Feynman one loop diagram with the fermions in the loop, that is the SM Higgs can talk to the SM particles through an effective coupling kappa ($\kappa_{ggh/\gamma\gamma h}$). For H, it can couple to h through effective interaction, β_g, and further couples to fermions through $y_{ttH/bbH}$, these couplings are chosen because their decay rate is dominant.

Writing down the Lagrangian for the interactions:

$$\mathcal{L}_{gg\phi} = -\frac{1}{4}\kappa_{ggh} G_{\mu\nu b} G^{\mu\nu b} h - \frac{1}{4}\kappa_{ggH} G^b_{\mu\nu} G^{\mu\nu b} H, \tag{3.50}$$

$$\mathcal{L}_{\gamma\gamma\phi} = -\frac{1}{4}\kappa_{\gamma\gamma h} F_{\mu\nu} F^{\mu\nu} h - \frac{1}{4}\kappa_{\gamma\gamma H} F_{\mu\nu} F^{\mu\nu} H. \tag{3.51}$$

In our choice of a 2HDM, $\kappa_{gg\phi}$ and $\kappa_{\gamma\gamma\phi}$ are given as

$$\kappa_{ggh} = \frac{\alpha_s}{3\pi v}\frac{3}{4}\mathcal{F}_{12}\left[\left(\frac{m_h}{2m_t}\right)^2\right], \kappa_{\gamma\gamma h} = \frac{e^2}{4\pi^2 v}\frac{47}{18}\mathcal{S}_{12}\left[\left(\frac{m_h}{2m_W}\right)^2, \left(\frac{m_h}{2m_t}\right)^2\right], \tag{3.52}$$

$$\kappa_{ggH} = \beta_g^H \frac{\alpha_s}{3\pi v}, \kappa_{\gamma\gamma H} = \beta_\gamma^H \frac{e^2}{4\pi^2 v}. \tag{3.53}$$

The functions $\mathcal{F}_{12}$ and $\mathcal{S}_{12}$ are found with a general functional form given as [8]:

$$\tau[1 + (1-\tau)f(\tau)] \to \tau[\zeta^\phi + (1 - \tau\zeta^\phi)f(\tau)], \tag{3.54}$$

where $\zeta^{\phi} = 1$ for $\phi = h, H$, and τ is the ratio of masses of particles involved in a one-loop calculation.

The new scalars (H and χ) lead to new interactions, where these new interaction arise from the effective couplings. The full Lagranian of the SM, including the Madala hypothesis, is written as:

$$\mathcal{L} = \mathcal{L}_{SM} + \mathcal{L}_{BSM}, \tag{3.55}$$

where

$$\mathcal{L}_{BSM} = \mathcal{L}_H + \mathcal{L}_Y + \mathcal{L}_T + \mathcal{L}_Q. \tag{3.56}$$

The $\mathcal{L}_Y, \mathcal{L}_T, \mathcal{L}_Q$ and $\mathcal{L}_H$, are the Yukawa, trilinear and quartic interactions of the scalar sector, which are defined as:

$$\mathcal{L}_H = -\frac{1}{4}\beta_g \kappa^{SM}_{hgg} G_{\mu\nu} G^{\mu\nu} H - \beta_V \kappa^{SM}_{hVV} V_\mu V^\mu H, \tag{3.57}$$

$$\mathcal{L}_Y = -\frac{1}{\sqrt{2}}[y_{ttH} t\bar{t}H + y_{bbH} b\bar{b}H], \tag{3.58}$$

$$\mathcal{L}_T = -\frac{1}{2}\nu[\lambda_{Hhh} Hhh + \lambda_{h\chi\chi} h\chi\chi + \lambda_{H\chi\chi} H\chi\chi], \tag{3.59}$$

$$\mathcal{L}_Q = -\frac{1}{2}\lambda_{Hh\chi\chi} Hh\chi\chi - \frac{1}{4}\lambda_{HHhh} HHhh - \frac{1}{4}\lambda_{hh\chi\chi} hh\chi\chi - \frac{1}{4}\lambda_{HH\chi\chi} HH\chi\chi. \tag{3.60}$$

The κ factors are the SM-like couplings, with $\kappa^{SM}_{hgg} = \alpha_S/(3\pi\nu)$ and $\kappa^{SM}_{hVV} = m_V^2/\nu$, where ν is the vacuum expectation value. The $\beta_g = y_{ttH}/y_{tth}$ is the scale factor with respect to the SM Yukawa top coupling, y_{tth}, and is used to tune the effective ggH coupling. β_V is similarly used for VVH coupling.

In the Madala hypothesis there is another heavy scalar, S, which is a scalar mediator. This scalar serves as a portal from the SM particles to the DM candidate.However, S boson is not present in the 2HDMs. S, in particular, is a key element in the hypothesis, since it acts as a portal to DM interactions through its $S \to \chi\chi$ decay[29]. The Madala hypothesis has been explained by an effective theory, however, the problem arises at the $Hh\chi\chi$ coupling. The branching ratio, $H \to h\chi\chi$ mode of a 3-body decay is large and it is not natural. To solve this, we introduce a singlet scalar S in the vertex of the $H \to h\chi\chi$ decay. The S boson mass has been chosen to be in the range $m_h < m_S < m_H - m_h$ and it is assumed to be produced mainly through the decay $H \to Sh$ with respect to $H \to hh$ [30]. The reason for introducing S is that, when we study H, it is allowed to have a decay mode, $H \to h\chi\chi$ and $H \to SS$ where

h is the SM Higgs boson and χ is the DM candidate, however, studies [30] found that the branching ratio for this decay mode should be large to explain current data, but it is not normal for a 3-body decay to have a large branching ratio and therefore the S boson was fit as an effective vertex. The S boson is kinematically accessible through the H decays, that is, $H \to SS, Sh, hh$ and it has Higgs-like couplings to the SM and suppressed production [30].

To include the effective interaction of the scalar particle, S, which opens up new possibilities in terms of search channels and phenomenology, we shall define several new vertices. An important feature to note is that all decay modes of S are possible, that is, S decays into leptons, vector bosons, DM and jets:

$$\mathcal{L}_S = \mathcal{L}_K + \mathcal{L}_{SVV'} + \mathcal{L}_{Sf\bar{f}} + \mathcal{L}_{hHS} + \mathcal{L}_{S\chi}, \tag{3.61}$$

where

$$\mathcal{L}_K = \frac{1}{2}\partial_\mu S \partial^\mu S - \frac{1}{2} m_S^2 SS, \tag{3.62}$$

$$\begin{aligned}\mathcal{L}_{SVV'} = &\frac{1}{4}\kappa_{Sgg}\frac{\alpha_S}{12\pi\nu} S G^{a\mu\nu} G^a_{\mu\nu} + \frac{1}{4}\kappa_{S\gamma\gamma}\frac{\alpha}{\pi\nu} S F^{\mu\nu} F_{\mu\nu} \\ &+ \frac{1}{4}\kappa_{SZZ}\frac{\alpha}{\pi\nu} S Z^{\mu\nu} Z_{\mu\nu} + \frac{1}{4}\kappa_{SZ\gamma}\frac{\alpha}{\pi\nu} S Z^{\mu\nu} F_{\mu\nu} \\ &+ \frac{1}{4}\kappa_{SWW}\frac{2\alpha_S}{\pi S_W^2 \nu} S W^{+\mu\nu} W^-_{\mu\nu},\end{aligned} \tag{3.63}$$

$$\mathcal{L}_{Sf\bar{f}} = -\sum_f \kappa_{Sf}\frac{m_f}{\nu} S f\bar{f}, \tag{3.64}$$

$$\mathcal{L}_{hHS} = -\frac{1}{2}\nu[\lambda_{hhS} hhS + \lambda_{hSS} hSS + \lambda_{HHS} HHS + \lambda_{HSS} hhS + \lambda_{HhS} hhS], \tag{3.65}$$

$$\mathcal{L}_{S\chi} = -\frac{1}{2}\nu\lambda_{S\chi\chi} S\chi\chi - \frac{1}{2}\lambda_{SS\chi\chi} SS\chi\chi. \tag{3.66}$$

In the Madala hypothesis we have introduced the hypothetical scalars H and χ to study the p_T spectrum of h, via a process $pp \to H \to h\chi\chi$. The brannching ratio for this process may be large or small depending on the coupling of $Hh\chi\chi$. This led to the introduction of another scalar, S, which explains the large branching ratio. This result in the couplings hHS, where $S \to \chi\chi$ and HSS, where $H \to SS$.

In the next chapter we review the theoretical and experimental constraints on 2HDM. The Madala hypothesis is based on the study of the 2HDM, as we have reviewed it, and now we review how these theory can be constarained both theoretically and experimentally. We have considered the heavy singlet scalar boson as it connects the SM-like Higgs boson and the DM to the heavy Higgs boson.

Chapter 4

Constraints on the 2HDM

Any model in particle physics has several parameters, our aim is to study how these parameters are constraint theoretically and experimentally within the 2HDM. In theoretical constraints, we shall talk about the boundedness of the potential and the unitarity. Also in experimental constraints, we talk about the flavour constraints as a result of a charged Higgs boson. We keep in mind that the SM serves as a basis when it comes to constraining any model in particle physics, their parameters should be constraint first before we could constraint any model of our choice.

4.1 Theoretical Constraints

The stability of a vacuum configuration is ensured by the positivity of the Higgs potential for large values of the field. The existence of a stable minimum allows us to perform perturbative calculations, and this condition requires also that the quartic terms of the potential be positive, i.e $\lambda_i > 0, i = 1, 2, 3, 4, 5, 6, 7$ where λ_i is a quartic coupling. For the 2HDM potential all the possible directions which the fields Φ_1 and Φ_2, the scalar potential is bounded from below if the following conditions are satisfied [31]:

$$\lambda_1 \geq 0, \qquad \lambda_2 \geq 0, \qquad \lambda_3 \geq -\sqrt{\lambda_1 \lambda_2}, \qquad \lambda_3 + \lambda_4 - \lambda_5 \geq -\sqrt{\lambda_1 \lambda_2}, \tag{4.1}$$

where λ_5 has been taken to be real and $\lambda_6 = \lambda_7 = 0$. These are actually necessary and sufficient conditions to ensure the positivity of the quartic potential along all directions, where these conditions have been obtained through a tree-level analysis.

Unitarity is the conservation of probability. When unitarity is violated this leads to violation of the principles of quantum mechanics. Therefore tree-level unitary constraints are preserved in a variety of scattering processes, which are scalar-scalar scattering, gauge boson-gauge boson scattering and scalar-gauge boson scattering, and the scalar potential must be bounded from below. The unitarity limit can be assured by the fact that $\Gamma_h \approx m_h$ [32], so that the physical Higgs boson disappears and the strong interactions in the Higgs sector is realised as strong interactions of longitudinal components of the gauge bosons [32]. In the 2HDM if λ exceeds the tree-level unitarity limitation, the observable Higgs particle would be meaningless [32]. Therefore, the correspondence amongst the tree level unitarity constraint realisation of the Higgs field and a possible strong interaction of the gauge bosons can generally be violated in the 2HDM if values of $\lambda_i,\ i = 1, 2, 3, ...$ differ from each other. Due to the richer scalar spectrum many scattering amplitudes need to be taken into consideration and the existence of the many quartic couplings makes things more complicated. This leads to the analysis of the eigenvalues of the S-matrix for scalar-scalar scattering amplitudes, and the relevant ones are given as follows [33]:

$$a_\pm = \frac{3}{2}(\lambda_1 + \lambda_2) \pm \sqrt{\frac{9}{4}(\lambda_1 - \lambda_2)^2 + (2\lambda_3 + \lambda_4)^2}, \tag{4.2}$$

$$b_\pm = \frac{1}{2}(\lambda_1 + \lambda_2) \pm \frac{1}{2}\sqrt{(\lambda_1 - \lambda_2)^2 + 4\lambda_4^2}, \tag{4.3}$$

$$c_\pm = \frac{1}{2}(\lambda_1 + \lambda_2) \pm \frac{1}{2}\sqrt{(\lambda_1 - \lambda_2)^2 + 4\lambda_5^2}, \tag{4.4}$$

$$e_1 = \lambda_3 + 2\lambda_4 - 3\lambda_5, \tag{4.5}$$

$$e_2 = \lambda_3 - 3\lambda_5, \tag{4.6}$$

$$f_+ = \lambda_3 + 2\lambda_4 + 3\lambda_5, \tag{4.7}$$

$$f_- = \lambda_3 + 3\lambda_5, \tag{4.8}$$

$$f_1 = \lambda_3 + 2\lambda_4, \tag{4.9}$$

$$p_1 = \lambda_3 - 2\lambda_4. \tag{4.10}$$

$$\tag{4.11}$$

The requirement of tree-level pertubative unitarity leads to:

$$|a_\pm|, |b_\pm|, |c_\pm|, |f_\pm|, |e_{1,2}|, |f_1|, |p_1| < 8\pi.$$

Further constraints includes the experimental constraints in 2HDM. We discuss how some branching ratios can constraint the mass of the charged Higgs boson.

4.2 Experimental Constraints

We have discussed the FCNCs constraints in the 2HDM in section 3.3, they are suppresed by introducing the Z_2 symmetry. In this section, we shall discuss how the 2HDM is constrained experimentally, in particular, we shall discuss the constraints on the charged Higgs sector due to the $b \to s\gamma$ and the $b \to \tau\nu$ processes. Note that all of these constraints are independent of the neutral sector.

The $(b \to s\gamma)$ branching rate was found to constrain the charged Higgs boson masses by excluding the lower masses, where at leading order (LO), it is given by [34]:

$$\mathcal{B}(b \to s\gamma) = \frac{|V_{ts}^* V_{tb}|^2}{|V_{cb}|^2} \frac{6\alpha_{e.m.}}{\pi g(z)} |C_7^{(0)eff}(\mu_b)|^2 \times \mathcal{B}(b \to ce\bar{\nu}_e). \tag{4.12}$$

The first factor is the ratio of CKM matric element, $g(z = m_c^2/m_b^2)$ is a phase space factor, and $C_7^{(0)eff}(\mu_b)$ is an effective Wilson coefficient, evaluated at the B-meson scale, μ_b. This effective Wilson coefficient is obtained from the relevant ones at the electroweak scale, $C_i^{(0)eff}(\mu_b)$, $i = 2, 7, 8$, [35] where the effects of the 2HDM enter. Certain linear combinations are denoted "effective" coefficients, as they are defined such that, for example, $C_7^{(0)eff}(\mu)$ includes all one-loop contributions to $b \to s\gamma$, and the four-quark operators [35]. The effective Wilson coefficient is sensitive to the scale of the B- meson decay, it changes by $\pm 25\%$, if the scale μ_b is varied by a factor of two in either direction around $m_b \simeq 5$ GeV [36].

The constraints on the charged Higgs parameters from the flavour physics depend strongly on the 2HDM Yukawa type, while others are type-independent. In type II and X models, a $\tan\beta$-independent lower limit is obtained from the $b \to s\gamma$ constraint [37]. At low $\tan\beta$ the constraints are similar among all Yukawa types as the Higgs couplings to up-type quarks are universal. For all types, the values of $\tan\beta < 1$ are ruled out for all values of high mass of the charged Higgs boson ($m_{H^\pm} > 650$ GeV), which includes the interesting non-decoupling region of the type I model [37].

There are several observables which probe mainly the type II model at high $\tan\beta$, with the most sensitive one being the $b \to \tau\nu$. There is a correlation between this mode (and several other, similar leptonic decays) and direct searches for $H^\pm \to \tau\nu$ since the same couplings enter the dominant 2HDM contribution. The very strong constraint from the branching ratio $(b \to s\gamma)$ is due to the contribution from the charged Higgs boson, which enters at the same level as the W boson contribution in the SM. The Wilson coefficient C_7 depends on the Yukawa couplings λ_t and λ_b.

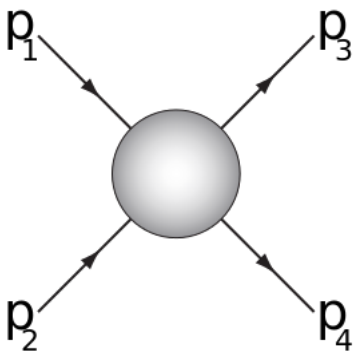

Figure 4.1: Mandelstam variables[41]

Since the Yukawa types, II and X share the same coupling pattern for the quarks, $|\lambda_{tt}| = 1/|\lambda_{bb}|$, one obtains a $\tan\beta$-independent lower limit on the charged Higgs mass for two types from the branching ratio of $(b \to s\gamma)$ [37]. The LEP experiments have constraints on the mass of the charged Higgs boson, it is set a lower limit on the $m_{H^\pm} > 78.5$ GeV at 95% confidence level [38]. The 2HDMs also has constraints in the flavour physics observables, precisely from the B meson decays. The constraints arises from the branching ratio of $B_s \to \mu^+\mu^-$ decay in the $m_{H^\pm} - \tan\beta$ plane, with $m_{H^\pm} > 80$ GeV and for values of $\tan\beta$, this can be seen in the LHC [39].

At the LHeC there is a flavor violation of $h, H \to b\bar{s}$ in the final states. This can be seen in the leptonic-specific model assuming a four texture in the Yukawa matrices and a general Higgs potential [40]

We shall now consider at some of the terminologies that are used in particle physics, wherein the next section we shall discuss the observables we measure at colliders and how we measure them at different colliders.

4.3 Collider Constraints

The importance of colliders is to help us verify the laws of fundamental physics and to understands the constraints of any model that attempts to predict nature. Firstly We shall explain some observables in colliders and then finish with how we can study constraints in colliders. The centre of mass energy: which tells the scale we are probing in and, type: e^+e^-, pp, $p\bar{p}$, e^-p. The centre of mass energy is the combination of the two particle beams which collide together. To talk about the centre of mass energy we should also talk about the energy squared of momentum, which is composed of two important parameters, the masses of the particles and the momenta, this is also refered as the Mandelstam variables:

$$
\begin{aligned}
s &= (p_1 + p_2)^2 = (p_3 + p_4)^2, \\
t &= (p_1 + p_3)^2 = (p_2 + p_4)^2, \\
u &= (p_1 + p_4)^2 = (p_2 + p_3)^2.
\end{aligned} \tag{4.13}
$$

These are Lorentz invariant quantities which are used in scattering processes, p_1 and p_2 are the incoming four-momenta and p_3 and p_4 are the outgoing four-momenta which converts the energy and momentum in a scattering process. The total centre of mass energy can also be defined as:

$$
E_{CM} \equiv \sqrt{s} \approx \begin{cases} 2E_1 \approx 2E_2 & \vec{p_1} + \vec{p_2} = 0, \\ \sqrt{2E_1 m_2} & \vec{p_2} = 0. \end{cases} \tag{4.14}
$$

When $\vec{p_1} + \vec{p_2} = 0$, we are in the centre of mass energy frame, which are suppoed to reach higher threshold and the $\vec{p_2} = 0$ are fixed target center of mass energy frame

When we collide particles in a collider environment we define our initial states appropriately and scatter the two beams of particles together. We are more interested in calculating the cross-sectional area of the particles, the branching ratios and the decay rates, which contain a lot of the physics in collider experiments. In particle physics we talk about the rapidity of the particles. The definition of the rapidity of a particle is:

$$
y = \frac{1}{2} \ln \left(\frac{E + p_z c}{E - p_z c} \right). \tag{4.15}
$$

This quantity is important because the rapidity, together paired with the azimuthal angle ϕ, (which is the angle a particle has been emitted at), there is an angular separation of two events, $(y_2 - y_1, \phi_2 - \phi_1)$ which is invariant with respect to boosts along the beam axis, where the axis of collision is taken to be the z-axis. The only problem with rapidity is that it can be very hard to measure for high relativistic particles, however, this leads us to define a quantity that is the same as the rapidity, that is pseudorapidity. Pseudorapidity is the spatial coordinate which describes the angle of a particle relative to the beam axis, where this is easier to measure for high energy particles than the rapidity. The definition of the pseudorapidity of a particle is:

$$
\eta = -\ln \tan \frac{\theta}{2}, \tag{4.16}
$$

where θ is the angle between the particle's momentum and the positive direction of the beam axis. This quantity is useful in hadron colliders where η can be measured more easily and quickly[42]. In LHC, we can measure this parameter very clearly and helps us to find the properties of the Higgs boson as they help us visualise the collider, however, we can change back to other colliders such as LHeC as we shall discuss in chapter 5

The other important quantity we should also mention is the luminosity for the collider, which is the number of particles passing each other per unit time through a unit transverse area at the interaction point. The maximum luminosity and the instantaneous number of interactions per second are referred to as the integrated luminosity.

In the next discussion, we shall mention the capabilities of the LHC experiment and the proposed ILC. The LHC experiment collides pp and it is responsible for the discovery of the Higgs boson. The ILC will focus on e^+e^- collisions and is referred to as a precision machine, as it shall collide individual particles which will produce a clean background [5]. Finally, we shall talk about the Large Hadron electron Collider (LHeC), which is proposed to collide electrons and protons and shall be the main concern of this work.

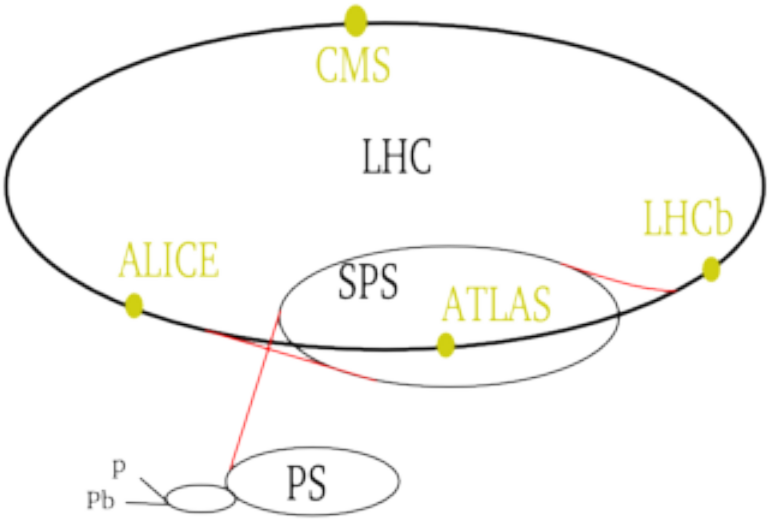

Figure 4.2: The Large Hadron Collider[43]

4.3.1 Large Hadron Collider

The LHC, as shown in Figure 4.2 is an up and running particle collider which collides protons together. The advantages of the LHC experiment is to enable us in investigating systematically the electroweak symmetry breaking, to study QCD and probe new physics beyond the SM.

Colliders are machines that help us in discovering of fundamental particles and testing theories thereof. The run-I of the LHC was at 7 TeV and can reach energies up to 13 TeV in the run-II [44]. Protons have strong interaction, and thus hadronic reaction yields large cross-sections. At higher energies, there are many possible channels that give resonance productions for different charge and spin states, induced by the initial parton combination such as $q\bar{q}$, qg, gg, there are also contributions like initial state WW, ZZ and WZ fusion, at the LHC the main production process are gluon fusion of producing a Higgs boson.

We shall consider the phenomenology of the 2HDM Higgs particle spectrum, where we shall focus on the CP-even scalars. We are interested in the study of the production and the decay of the CP-even scalars and its couplings. The phenomenology of the SM-like boson in the 2HDM is similar to that of the SM Higgs boson, the vector boson coupling constants for the SM-like boson, hZZ and hW^+W^- are given by the SM Higgs are proportional to $\sin(\beta - \alpha)$, while those for HZZ and HW^+W^- are proportional to $\cos(\beta - \alpha)$. These vertices are important for phenomenology, as it is important to note that the CP-even particles share the Higgs field vev and

Table 4.1: *Couplings of h^0 and H^0 to gauge bosons pairs:*

$\cos(\beta-\alpha)$	$\sin(\beta-\alpha)$
HW^+W^-	hW^+W^-
HZZ	hZZ
ZAh	ZAH
$W^\pm H^\mp h$	$W^\pm H^\mp H$
$ZW^\pm H^\mp h$	$ZW^\pm H^\mp h$
$\gamma W^\pm H^\mp h$	$\gamma W^\pm H^\mp h$

the strength of the coupling of the W^+W^- and ZZ to scalar fields. Furthermore, the decay of the Higgs boson in the 2HDM depends on the model for the Yukawa interaction and also $\sin(\beta-\alpha)=1$ which is the alignment limit. The decay pattern of h is almost the same as that of the SM. However the decay of H can vary over a large range of $\tan\beta$.

In the phenomenology of the 2HDM particle spectrum, the couplings of the Heavy and lighter Higgs as summarised in table 4.1. Furthermore, the decay of the Higgs boson in the 2HDM depends on the model for the Yukawa interaction, and the decay of H can vary over a large range. As such, we have conducted a general scan for an additional heavy Higgs boson, $H \to \gamma\gamma$, in a mass range between $2m_h < m_H < 2m_t$ [8].

4.3.2 2HDM CP-even scalars study in the LHC

In 2HDMs we obtain five Higgs boson after EWSB, the two CP-even scalars, the charged Higgs and CP-odd scalars, as we have detailed in chapter 3. Our focus in this dissertation is the CP-even scalars. These CP-even scalars have spin zero and are neutral, and because of the alignment limit, they have different couplings and masses. The light Higgs boson is taken to be the SM-like Higgs boson because it is compatible with the properties of the SM Higgs boson, that is, the couplings and masses are set to be the same.

The light Higgs boson has a production at the LHC and proceeds through gluon fusion (ggF), vector boson fusion (VBF), and the associated production of the Higgs with gauge boson (Vh) and associated with top quark pairs.

There are several decay channels that the light Higgs boson can have, the most dominant one is a pair of bottom quarks, and this arises in the ggF or the VBF. However, this decay channel is very difficult to detect for the light Higgs boson,

because of the presence of large backgrounds [45]. An alternative way is to require leptons in the final states, from the associated production of the Higgs boson with gauge bosons or a pair of top quarks, which helps to reduce the background [45].

The heavy Higgs can also be produced at the LHC, with a mass at or below 1 TeV. The heavy Higgs can also decay into electroweak gauge bosons and quarks, including the discovered Higgs boson. When the branching ratio of the heavy Higgs has one or more light Higgs bosons, it dominates when kinematically accessible [45].

The dimensionless coupling strengths of ζ_H^f, with $f = u, d, l$, and H a neutral Higgs boson are listed in the table 3.1, for the various types of 2HDMs. In the alignment limit, all dimensionless Yukawa coupling of ζ_H^f are inversely proportional to $\tan\beta$. With the low-$\tan\beta$ inputs, the heavy Higgs always couple strongly to the top quark [46]. Though we focus on the alignment limit of $\cos(\beta - \alpha) = 0$, it is noted that the CP-even Higgs boson h in the 2HDM generally allows the parameter choice of $\cos(\beta - \alpha) \sim \mathcal{O}(0.1)$ [47].

There are two scenarios we can look at for a heavy Higgs, when the mass is below the top quark pair production threshold and when the mass is above the top quark pair production threshold. The former has the dominating $H \to hh$ over competing Yukawa decays to bottom quark pairs [48] and the latter has decays that are comparable in rate to decays into top quark pairs and are more distinctive [48].

The CP-even h and H couples at tree-level to a pair of W and Z bosons and a pair of fermions, and at one-loop to $gg, \gamma\gamma$ and $Z\gamma$ similar to the SM Higgs boson. As a result, A which is CP-odd does not couple to a pair of W's or Z's. For the same reason, it will not couple to a pair of hh, hH or HH. The A boson can couple to a pair of fermions. At loop-level, the CP-odd A will couple to $gg, \gamma\gamma$ and $Z\gamma$, just as h and H would.

Since the $H \to hh$ has a dominant branching ratio, it is interesting to look at the final state for this dominating branching ratio. The final states used in this search consist of charged leptons, or a resonant photon pair accompanied by at least one charged lepton (charged leptons are e, μ, τ or hadronic decays of the τ-leptons τ_h).

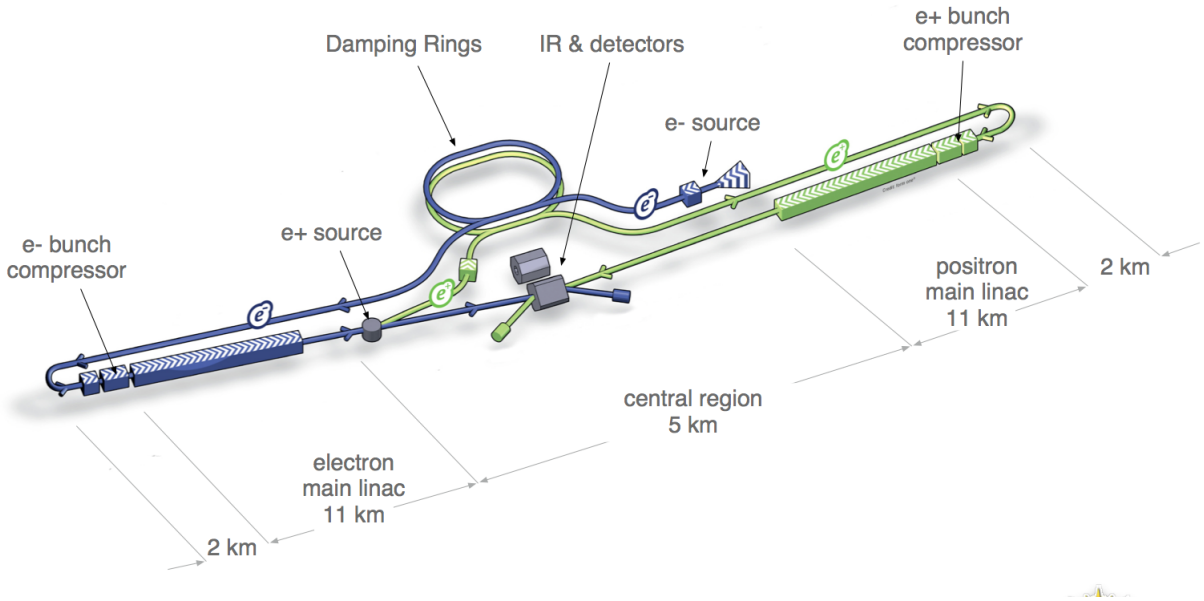

Figure 4.3: The International Linear Collider overview layout [49]

4.3.3 International Linear Collider

The ILC as shown in Figure **??** is a proposed linear particle collider, which is planned to collide electrons and positrons with an initial centre of mass energy of 500 GeV, and later an upgrade to 1 TeV. The objective of the ILC is to describe the system of measurements that will be capable of probing the Higgs boson, such as the Higgsstrahlung process ($e^+e^- \to Zh$), the W-fusion process ($e^+e^- \to v_e\bar{v}_e h$), and the Z-fusion process ($e^+e^- \to e^+e^- h$) [5]. These will also enable us to identify the major Higgs decay, $h \to b\bar{b}$. With the Higgsstrahlung we would obtain the maximum cross-section, where this also has the advantage of allowing us to also identify the Z boson at a well-defined energy corresponding to the kinematics of the recoil against the Higgs boson. As such it would also be possible to identify the Higgs events without looking at the Higgs decay [50].

The other advantage of the ILC is that it provides a cleaner background environmental and the reconstruction can be made easily. Hence the important continual background source comes from the photon-photon ($\gamma\gamma \to \gamma\gamma$) [5]. The cross-section is thus around few hundreds nb (nano-barn). This experiment will play a compatible role in clarifying the properties of the elementary particle.

The e^+e^- environment thus provides a setting in which a basic high-energy collision can be measured with high precision [5]. The Higgs events occur at about 1% of all e^+e^- annihilation, and the resulting events are quite interesting. At the

ILC the initial state e^+ and e^- are pointlike elementary particles, and there is a drastic improvement in the accuracy of the coupling determination. The ILC shall also provide polarised electron and positron beams [51].

The ILC will be set to a centre of mass energies at 91 GeV and 160 GeV, these energies will correspond to the Z resonance.These energies are set by the ILC and are the threshold for $e^+e^- \to W^+W^-$ [49]. The ILC is capable of archiving a luminosity much higher, at the energy 250 GeV. The reaction $e^+e^- \to Zh$ will reach the peak cross-section at energies $250 - 1000$ GeV. The annihilation cross-section is expected to show a prominent rise associated with the threshold for the top quark pair production at 500 GeV. At this energy and high luminosity, the ILC is expected to increase the power of the precision measurements. The ILC will also allow for the search of new particles at 1 TeV. These higher-energies at the ILC enables a number of new measurements sensitive to the Higgs boson coupling to the top quark and Higgs self-coupling [51].

The goal of the ILC is to search for the extended Higgs sector by making precise measurements, as it will be easier compared to the LHC to access the properties of the Higgs particle. That is it will study the properties of the discovered Higgs boson at the LHC and opens doors to explore NP.

In the next chapter, we shall review the LHeC, by first looking at how it will be constructed and the possible detector set up. We shall also review the elastic and inelastic scatterings which will serve as a layout to chapter 6, we shall study the CP-even scalars in the LHeC.

Chapter 5

The Large Hadron electron Collider

The LHeC programme is a proposed upgrade that shall operate after the LHC programme is finished [52]. The LHeC provides the only realistic possibility for an energy frontier *ep* programme of experimentation in the coming decades, where it shall collide beams of electrons and protons together with different energies. What makes the LHeC so interesting is that the initial states are asymmetric, and hence backward and forward scattering can be disentangled. It also provides a clean environment with suppressed backgrounds from strong interaction processes [53].

The electron beam in the LHeC tunnel would allow us to achieve an outstanding luminosity of about $10^{33} cm^{-2} s^{-1}$ in the *ep* interactions [54]. The LHeC is planning to build a different type of collider to the LHC. That is, it will have extra features compared to the LHC, such as, the "ring-ring" (RR) which will be responsible for proton configuration and the "linac-ring" (LR) which will be responsible for the electron configuration. However, such a ring may be built without any major technical obstacles. For the comparison of RR and LR option, E_e was kept the same at 60 GeV. The ring could extend to somewhat higher energies, but only a Linac would allow 100 GeV to be significantly exceeded. The potential for higher energy is not the only, and possibly not the dominant reason, for considering a linac-ring collider. Other important benefits include the potential for higher electron current than assumed in the LHeC baseline design, and thus higher luminosity [51].

A choice between the two configurations, RR and LR, is envisaged to be taken soon after the appearance of the conceptual design report (CDR). It is important to consider that the RR configuration delivers high electron luminosity, with diffi-

culties for high polarisation. While the LR configuration has a high potential for polarised electrons. The electrical power required for the RR collider at a constant beam current increases with the fourth power of energy, while for the LR collider the increase is roughly linear as long as the synchrotron radiation loss in the return arcs remains a small fraction of the total [55]. For higher electron energies in the ring, the polarisation greatly decreases, whereas for the linac solution the polarisation is independent of the beam energy. A choice of one over the other option has to be based on physics but also technical, cost and further considerations.

The LHeC will be the second electron-hadron collider following HERA [56]. The LHeC physics programme demands a very high level of precision, as the measurement of the strong coupling constant α_s requires the reconstruction of complex final states, as appear in charged current Higgs production and decays into $b\bar{b}$ final states [57]. As a consequence of the asymmetric electron and proton beam energy configuration, the detector acceptance has to extend as close as possible to the beam axis. The dimensions of the detector are constrained by radial extension of the beam pipe, due to synchrotron radiation [53].

The LHeC will choose a default energy of the electron at $E_e = 60$ GeV and the proton at $E_p = 7$ TeV. At these energies, the LHeC will deepen our understanding of TeV scale physics, and the study of the NP. The LHC has excluded much of the sub-TeV physics beyond the SM, but leaves the possibility open of resonant lepton-parton states with masses of larger than about 700 GeV, for which the LHeC would be a particularly suitable machine with a range of up to $M \leq \sqrt{s}$ [53].

High precision QCD and electroweak physics require a maximum range of $\ln Q^2$ and highest Q^2(kinetic variable, and shall be discussed in section 5.1.1) [53], respectively. The unification of electromagnetic and weak force takes place at $Q^2 \simeq M_Z^2$, which is much exceeded with the LHeC energies. Part of the electroweak physics programme requires lepton beam polarisation, which is a ring configuration is difficult to achieve for energies higher than 60GeV. The discovery of gluon saturation requires us to measure at typical values of small Bjorken x, $x \simeq 10^{-5}$ with $Q^2 \gg M_p^2$, where M_p is the mass of the proton. The choice of these energies ensures this discovery at the LHeC in the deep inelastic scattering region [58]. Energy losses by synchrotron radiation are proportional to E_E^4, both in the ring and the return arcs for the linac, but can be kept at reasonable levels, in terms of the power, P, needed to achieve high luminosity, and the radius of the racetrack return arc can be chosen such that the LHeC tunnel in the linac configuration is only 1/3 of the LHC [53].

Thus it appears that 60GeV is an appropriate and affordable choice, and yet it is well possible that 60GeV may not be the final value of the electron beam energy, especially if the LHC would find non-SM physics just above the default energy range considered here. The design, therefore, also considers a dedicated high energy beam of 140GeV as an option [53].

There has often been a discussion about the need for two detectors and an ambitious detector push-pull concept [53]. For the LHeC this would imply a major overhead of cost and delay in construction time. The detector envisaged here will be challenging but also based on known technology. The detector shall be discussed further in section 5.2

5.1 Electron-Proton Scattering

There are two types of collisions (scattering) that we shall review, the elastic collision and the inelastic collision. Elastic collisions are a process in which the total kinetic energy of the system is conserved. The study of the inelastic collision helps in understanding the gluon field. This is achieved with precision measurements of the evolution of structure functions over an unprecedented range of $\ln Q^2$. It relates to inclusive ep deep inelastic scattering with jets and heavy flavour, it also concerns the unexplored role of the gluon in nuclei and in deep virtual Compton scattering. The gluon field is central to QCD but not directly measurable. It may exhibit spots of maximum density (hot spots) and it may also dissapear (cold spots) as it does towards low Q^2 and x, and possibly at the scaling point near $x \approx 0.2$. The gluon helps in the understanding of the origin of baryonic matter, where we explain more on parton densities in Appendix B. The production of the Higgs bosons and of other new particles and, not least important, understanding QCD.

We shall emphasise more on Rutherford scattering, Mott scattering and Rosenbluth scattering formulae. Inelastic collisions are processes in which the total kinetic energy of the system is not conserved, that is, some of the energy is lost or transferred between particles. We shall discuss about deep inelastic scattering, which is the breaking up of the protons into its constituents particles, where some of the kinetic energy is lost to the vibration of the proton during scattering Our goal for this section is to understand how the electrons and protons collide.

One of the most useful tools to study the structure of the proton is the electron-proton scattering, where we can probe the unknown structure of the proton with

the electron, which can be very well studied with QED. It is clear that to reveal the structure of the proton on some scale depends on the energy of the probe, in our case the electron. The higher the energy the finer the structure probed.

We shall discuss about how we scatter two different types of particles, the electrons and the protons, with different energies, but our starting point is to look at the relationship between wavelength (λ) of the photon and the radius of a proton (r_p). Hence the ratio of the wavelength to the proton gives us an important phenomena and plays a huge role:

- At very low electron energies $\lambda \gg r_p$, the scattering is the same as the point-like particle. The electron has been scattered and it is non-relativistic.
- At low electron energies $\lambda \approx r_p$, the scattering is the same as to the extended charged object and relativistic effects of the electron have to be considered.
- At high electron energies $\lambda < r_p$, the wavelength is very short to penetrate the substructure, that is, scattering from constituents quarks. The cross-section of the elastic scattering becomes small and the dominant cross-section becomes that of the inelastic scattering.
- At very high electron energies $\lambda \ll r_p$, the proton appears to be a structure of quarks and gluons.

5.1.1 Elastic Scattering

To calculate the cross-section of the elastic scattering, we shall use the Rurtherford scattering formula. Here the electron has a low energy such that it can be treated as a non-relativistic particle. Also the proton can be treated as a point particle, and we can neglect the recoil of the proton. The differential cross section is:

$$\left(\frac{d\sigma}{d\Omega}\right) = \frac{\alpha^2}{16E_e^2 \sin^4(\theta/2)}, \tag{5.1}$$

where E_e is the electron energy, θ is the scattered angle and α is the fine structure constant.

Taking into account the spin of the electron, we get the Mott cross-section:

$$\left(\frac{d\sigma}{d\Omega}\right) = \frac{\alpha^2}{4E_e^2 \sin^2(\theta/2)} \cos^2\left(\frac{\theta}{2}\right). \tag{5.2}$$

In this case the electron is relativistic and we neglect the recoil of the proton with the spin interactions.

In the high energy regime we consider the proton recoil and the magnetic spin interation: To do so let us start with the momenta

$$\begin{aligned} p_1 &= (E_1, 0, 0, E_1) \\ p_2 &= (m_p, 0, 0, 0) \\ p_3 &= (E_3, 0, E_3 \sin\theta, E_3 \cos\theta) \\ p_4 &= (E_4, p_4). \end{aligned} \tag{5.3}$$

The mass of the electron is negligibly small and the matrix element for this process is as follows, where we show the explicit calculation in Appendix C:

$$\langle |\mathcal{M}_{fi}|^2 \rangle = \frac{8g^4}{(p_1 - p_3)^4} \Big[(p_1 \cdot p_2)(p_3 \cdot p_4) + (p_1 \cdot p_4)(p_2 \cdot p_3) - (p_1 \cdot p_3) m_p^2 \Big]. \tag{5.4}$$

The momemtum is conserved, and expressing the inner product in terms of E_1, and E_3 and θ,

$$\langle |\mathcal{M}_{fi}|^2 \rangle = \frac{8e^4}{(p_1 - p_3)^4} m_p E_1 E_3 \left[(E_1 - E_3) \sin^2\left(\frac{\theta}{2}\right) + m_p \cos^2\left(\frac{\theta}{2}\right) \right]. \tag{5.5}$$

Expressing in terms of the kinetic variable Q^2,

$$Q^2 \equiv -q^2 = -(p_1 - p_3) = 4E_1 E_3 \sin^2\left(\frac{\theta}{2}\right). \tag{5.6}$$

Therefore we can obtain the energy lost by the electron in terms of Q^2 as:

$$E_1 - E_3 = \frac{Q^2}{2m_p}. \tag{5.7}$$

We note that $Q^2 < 0$ and hence $E_1 - E_3 > 0$. The scattered electron is always lower in energy than the incoming electron. Writing the cross-section,

$$\left(\frac{d\sigma}{d\Omega}\right) = \frac{\alpha^2}{4E_1^2 \sin^2(\theta/2)} \frac{E_3}{E_1} \left[\cos^2\left(\frac{\theta}{2}\right) + \frac{Q^2}{2m_p} \sin^2\left(\frac{\theta}{2}\right) \right]. \tag{5.8}$$

The Mott cross-section is reffered to as the elastic scattering and is equivalent to the scattering of the spin half electron from a fixed electrostatic potential, the term E_3/E_1 is proportional to the proton recoil and the term $\sin^2(\theta/2)$ is proportional to the magnetic interaction due to the spin-spin interaction.

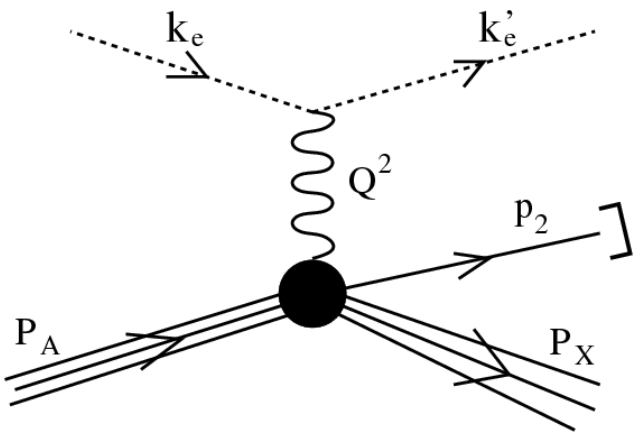

Figure 5.1: *Inelastic scattering, the p_A is the initial momentum of the proton and k_e is the initial momentum of the electron. The p_2 and p_X are the final momentum of the proton and the $k'_e$is the final momentum of the electron and the $Q^2$is the momentum transfer.*

Regarding the charge distribution and the magnetic moment in the proton, we introduce two structure funtions, $G_E^2(Q^2)$ and $G_M^2(Q^2)$, where we include them in the cross-sectional calculation, and thus it is now called the Rosenbluth scattering formula:

$$\left(\frac{d\sigma}{d\Omega}\right) = \frac{\alpha^2}{4E_1^2\sin^4(\theta/2)}\frac{E_3}{E_1}\left[\frac{G_E^2(Q^2)+\tau G_M^2(Q^2)}{1+\tau}cos^2\left(\frac{\theta}{2}\right)+2\tau G_M^2(Q^2)\sin^2\left(\frac{\theta}{2}\right)\right], \tag{5.9}$$

with τ is defined as,

$$\tau = \frac{Q^2}{4m_p^2}. \tag{5.10}$$

5.1.2 Inelastic scattering

In Figure 5.1 we show a Feynman diagram of deep inelastic of an electron-proton scattering, which can be a test for perturbative QCD. One of the aspects which is important in the deep inelastic scattering are the structure functions. They are used to predict the cross-section in high-energy hadron collisions. For the deep inelastic electron-proton scattering they help us to interpret the parton picture in terms of quarks and gluons in a hadron. There is a large momentum transfer, and this results in more than just electrons and protons in the final state and there is little scattering.

Let us consider the scattering of a high-energy electron off a proton, where we label the incoming and the outgoing electrons by k_e, k'_e, and the momentum of the proton by p_A. The momentum transfer can be labelled $Q^2 = k_e - k'_e$. The inelastic

scattering has additional Lorentz invariant kinematics, which is quantified by the variables x,Q^2,y,ν, note that these are not related. This results in the breaking up of the proton, compared to the kinematics of elastic scattering. The Bjorken x(this is a scale where particles that are experimentally observed are point-like when probed at high energy) measures the elasticity of the collision and can take any value between 0 and 1 [59]. For the case where $x = 1$ corresponds to elastic scattering and the final state is simply a proton. The measurement of x provides us with information about the way the momentum of the proton is distributed between the quarks, where we define the Bjorken x in terms of Q^2 as:

$$x \equiv \frac{Q^2}{2p_2 \cdot q}. \tag{5.11}$$

The kinematic variable y measures the inelasticity of a collision, and we define it as:

$$y \equiv \frac{p_2 \cdot q}{p_2 \cdot p_A}. \tag{5.12}$$

In the proton rest frame, y is the fractional energy lost by the electron and we write it as:

$$y = 1 - \frac{E_3}{E_1}. \tag{5.13}$$

This also shows that y takes values between 0 and 1. The kinematic variable ν is the energy lost by the electron, and it is defined as follows:

$$\nu = E_1 - E_3. \tag{5.14}$$

The scalar variables have the relation:

$$p_X = p_A + q$$

.

This leads to

$$p_X^2 = M^2 + 2p_A \cdot q + q^2, \tag{5.15}$$

where M is the mass of the proton. The invariant mass of the final state is expressed as:

$$W^2 = p_4^2 = (p_2 + q)^2. \tag{5.16}$$

This leads us to other scalar variables,

$$\begin{aligned} M\nu &= p \cdot q, \\ q^2 &= -Q^2, \end{aligned} \tag{5.17}$$

which gives us

$$2M\nu = Q^2 + W^2 - M. \tag{5.18}$$

This lead us to the same situation as in elastic scattering ,but now the structure funtions $G_E^2(Q^2)$ and $G_M^2(Q^2)$ are replaced by $F_2(x, Q^2)$ and $F_1(x, Q^2)$.

The next step is to construct the cross-section for the inelastic scattering. This cross-section shall be related to the cross-section for the electron-quark elastic scattering [60]. It is important to note the inelastic scattering is determined by quantities x and Q^2. The starting point is the Rosenbluth scattering formula Eqn. (5.9), and the electron-proton inelastic scattering mediated by a virtual photon [61]:

$$\left(\frac{d\sigma^2}{dxdQ^2}\right) \approx \frac{4\pi\alpha^2}{Q^4}\left[(1-y)\frac{F_2(x,Q^2)}{x} + y^2 F_1(x,Q^2)\right]. \tag{5.19}$$

The factors F_1 and F_2 are the structure functions, the y quantity in this expression is related to x and Q^2 by:

$$y = \frac{Q^2}{(s - m_p^2)x} \approx \frac{Q^2}{sx}, \tag{5.20}$$

where s is the centre-of-mass energy. Thus we can write the cross-section for the electron-quark scattering as:

$$\left(\frac{d\sigma}{d\Omega}\right) = \frac{4\pi\alpha^2 Q_q^2}{Q^4}\left[(1-y) + \frac{y^2}{2}\right]. \tag{5.21}$$

To study the CP-even scalars at the LHeC, the The LHeC detector will be one of the important central pieces of the LHeC programme. The design of the LHeC detector will be flexible, modular and affordable.

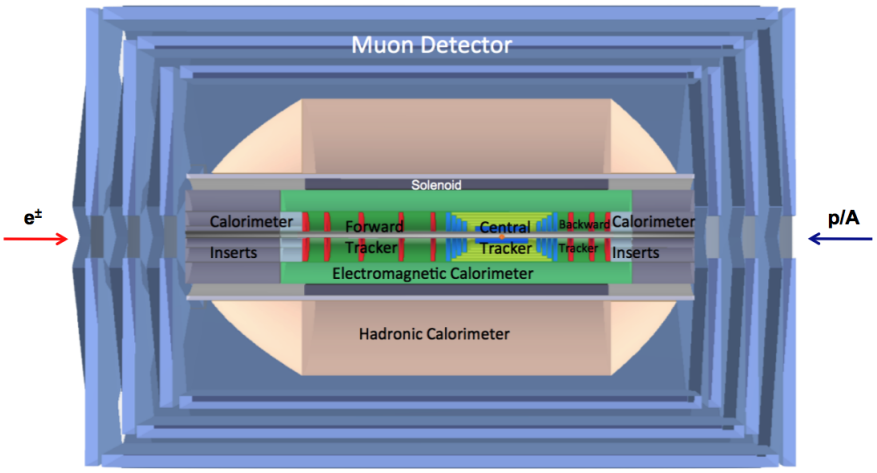

Figure 5.2: The proposed Large Hadron electron Collider detector [62]

5.2 Detector

In the central barrel shown in Figure 5.2, we shall consider the components of the detector, where, the silicon pixel which is in the centre, is surrounded by silicon tracking detectors; The particles (electrons and protons) will go through an electromagnetic calorimeter inside a 3.5 T solenoid and a dipole magnet with a 0.3 T field on axis. There will be a hadronic tile calorimeter for the solenoid flux for a head-on collision, this will track the inner momentum measurements [54]. The energy of the electron is measured in the backward calorimeter, and the electron is scattered into the silicon tracker.

To verify the design of the detector, the calorimeter performance and tracking simulation will be applied for verification [62]. The central tracker which the momentum resolution will be based on is $\delta p_t/p_t^2 = 6.10^{-4}$ GeV^{-1} and will translate to parameter resolution of 10μm, which will be combined with the beam spot of 7μm. There will be a heavy quark tagging environment in transverse directions [54].

The LHeC will have radiation level much lower than the LHC. The LHeC detector components will follow that of HERA [54]. The LHC gives us the upgrade and the time schedule of the LHeC project [54]. A study of the first installation was made considering pre-mounting the detector at the surface. The detector will be small enough to fit into the L3 magnet structure of 11.2m diameter, which would be available as mechanical support. Based on the design, as detailed in the CDR, it is estimated that the whole installation can be done in 30 months [54].

In the next chapter, we shall study the CP-even scalars in 2HDM. The aim is to

study the CP-even scalars in the LHeC and the Future Circular Collider for protons and electrons (FCC-he). The difference between the two colliders is that the LHeC has a fixed proton energy of $E_p = 7$ TeV and the FCC-he has a fixed proton energy of $E_p = 50$ TeV.

Chapter 6

Exploring two CP-even scalars in the LHeC

The production mechanisms in the LHC that are responsible for producing a Higgs boson in the SM are as follows: VBF, which is a process where the production Higgs boson via a tree-level process through the vector bosons $W^{\pm}, Z$ couplings; Gluon gluon fusion (ggF), possible top associated Higgs production, and vector boson associated Higgs production. We shall shift our focus to the LHeC, where we shall discuss the charged current (CC) process and the neutral current (NC) process as shown in Figure 6.1. The CC and the NC have the potential to increase the Higgs boson signal efficiency, and they are both studied with a forward jet tagging in Ref [63].

We shall study the Higgs boson decay to final state particles, such as $h \to b\bar{b}$ and $h \to \tau^{+}\tau^{-}$ (as these final states are interesting to study in the LHeC), as the Yukawa coupling to the other fermions are very difficult to access at the LHC. The LHeC can also investigate the hWW vertex which will provide insight into the nature of electroweak symmetry breaking. The LHeC uses DIS which we shall emphasise below, where this shall help us in probing inside the proton. We can classify the LHeC physics into categories which may overlap: *i*) The LHeC includes the study of the Higgs boson, top quark physics and beyond the SM theories, *ii*) It includes the deep inelastic scattering precision and gluon distribution, *iii*) the parton structure and perturbative QCD, *iv*) modified parton distribution functions (PDF)-these are defined as the per-nucleon structure-function ratio. We mention the PDF in detail in Appendix B. The most important subject we shall present in more detail is the Higgs physics at the LHeC, where we study the Higgs boson and the Madala boson in the next section.

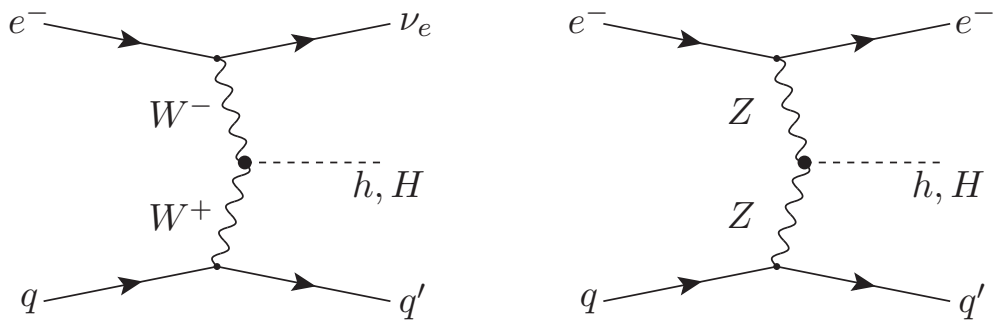

Figure 6.1: *Production modes of h and H through CC (left) and NC (right) in e^-p colliders through VBF. Here $q, q' = u, d, c, s, b, \bar{u}, \bar{d}, \bar{c}, \bar{s}, \bar{b}$.*

6.1 Production of the Madala boson in the LHeC

DIS which we studied in section 5.1.2, led us to the production of gauge bosons [54]. The Higgs particle is produced in the WW and ZZ fusion in the ep collisions at the LHeC. These production modes can be uniquely identified by the nature of the charged or neutral current process, and decays can be studied with low background, including the dominant decay to $b\bar{b}$. From the WW production, the contributions from CP-even or CP-odd Higgs quantum numbers can be extended. In this dissertation, we have calculated the heavy Higgs boson using the 2HDM framework inside the LHeC. The mass parameter choice of $m_H = 270$ is the Madala boson and it has been chosen according to Ref. [27], where the most important Yukawa couplings inside the 2HDM are the hVV ($V = W^{\pm}, Z$), and they depend on the choice of α and β parameters. For example, couplings for hW^+W^-, hZZ depend on $\sin(\beta-\alpha)$, while in the case of HW^+W^-, HZZ it is proportional to $\cos(\beta-\alpha)$. We produce the heavy Higgs boson and the SM-like boson inside a type II 2HDM.

The parameter regions where all the theoretical and experimental constraints are imposed shall be the starting for us, the first study of the $\tan\beta$ and $\sin(\beta-\alpha)$ dependence of the cross-section for the search channels, $e^-p \to e^-hj$ and $e^-p \to \nu hj$ at the LHeC. Fixing $m_h = 125$ GeV we have five more free parameters, three masses, $m_H, m_A, m_{H^{\pm}}$ and the two angles, which shall parameterise as $\tan\beta$ and $\sin(\beta-\alpha)$. Varying these parameters, we now study the remaining parameter regions satisfying all the theoretical and experimental constraints, as well as regions that are consistent with the observed Higgs signal.

Regions of $\sin(\beta-\alpha)$ and $\tan\beta$ are highly restricted once we require the light CP-even Higgs to be observed as the 125 GeV scalar particle, $\tan\beta$ between 0.5 to 4 for $\sin(\beta-\alpha)=\pm 1$, and $\tan\beta$ between 1.5 to 4 for $0.5<\sin(\beta-\alpha)<0.9$. The masses of the other Higgses, $m_H, m_A, m_{H^\pm}$, however, are largely unrestricted and uncorrected, except for the region where $\sin(\beta-\alpha)>0$ and $m_{A,H^\pm} \gtrsim 600$ GeV, which exhibits a strong correlation between these two masses. Flavour bounds do not change the allowed parameter space much except for the charged mass, which is constrained to be above 300 GeV. Imposing the flavour constraints leaves the regions with $m_{H^\pm} \gtrsim 300$ and $0.55<\sin(\beta-\alpha)<0.9$. LEP places a lower bound on the charged Higgs around 80 GeV [64]. Flavour bounds have expectations that the rule out any values of $m_{H^\pm} \lesssim 300$ GeV for all the values of $\tan\beta$, mainly due to the $b\to s\gamma$ constraint.

6.2 Discussion

In Figure 6.2 we provide a preliminary study of the cross section measurements of h and H using energies from the LHeC and FCC-he configurations. For $E_e = 60$ GeV and $E_p = 7$ (50) TeV the chosen parameters give substantial signal rates for H production in CC and NC modes are (with $m_H = 270$ GeV), $\sigma_H^{CC} \sim 2.2(11.3)$fb and $\sigma_H^{NC} \sim 0.38(3)$fb respectively. While for h production these rates are $\sigma_h^{CC} \sim 150(450)$fb and $\sigma_h^{NC} \sim 28(124)$fb. Here we considered e^- polarisation of -80%, which enhances the unpolarised signal cross sections (and also backgrounds) by 1.8 times.

In Figure 6.2 we also provide the study of the cross section measurements of h and H for a fixed electron energy $E_e = 60$ GeV from the LHeC with fixed proton energy $E_p = 7$ TeV and FCC-he with fixed proton energy $E_p = 50$ TeV. We have varied the mass of the Higgs SM-like Higgs boson and heavy Higgs boson in both CC channel and NC channel. We have used `Madgraph 5` to calculate the cross-section and it was set to `nn23lo1`.

We have also given estimations of the BRs, as shown in Table 6.1-6.2, for various decays of h, H, A and $H^\pm$, based on our parameter choice. For these parameter choices the dominant final state, such as, $H\to hh\to b\bar{b}b\bar{b}$ and thus at the LHeC/FCC-he one can estimate the sensitivity of Hhh couplings including the HW^+W^- and HZZ.

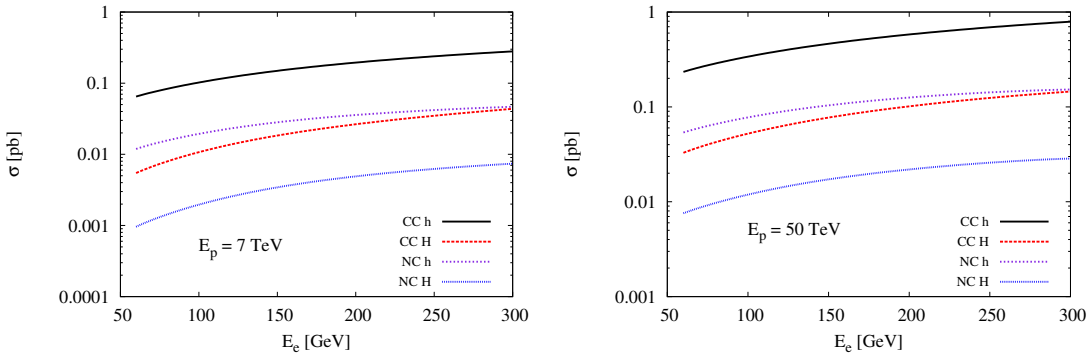

Figure 6.2: Production cross section of h and H in both CC and NC channels with respect to the electron beam energies E_e for fixed proton beam energy of $E_p = 7$ TeV and $E_p = 50$ TeV. The default model parameters are as explained in the text with $\tan\beta = 1.0$ and e^- polarisation is taken as -80%.

Here it is important to mention that the SM Higgs-boson BR to the $b\bar{b}$ mode has been studied, and tagging the forward jet assures this decay mode has a significantly reduced background which improves the purity of the signal [65]. Therefore, estimations of the BRs suggest $H \to hh \to b\bar{b}b\bar{b}$ as the dominant mode (which would be a signal rate of $\sim 55\%$ of the total production cross section of H, where the rate of one of the dominant backgrounds $b\bar{b}b\bar{b}j$ in the CC (NC) at the LHeC would be $\sim 2.0\ fb$ $(22\ fb)$, while for the FCC-he the cross section is around 3 (7.5) times higher for $E_e = 60$ GeV), while $H \to hh \to W^+W^-$ are subdominant signal modes. Hence the sensitivity of the Hhh, HW^+W^- and HZZ couplings in this mode can be measured at the LHeC/FCC-he [66].

We have calculated the production rates in the e^-p collider environment, which has been proposed by the LHeC/FCC-he. We have looked at different channels in producing the CP-even scalars. The NC channel $(e^-p \to e^-h^0/H^0j)$ and the CC channel $(e^-p \to \nu_e h^0/H^0 j)$. The theoretical model that we have focused on is the 2HDM, where the the CP-even scalars are the SM-like Higgs boson (h^0) and the heavy Higgs boson (H^0). We only show the 2HDM type-II cross section for both electron energy in Figure 6.2 and Higgs bosons mass in Figure 6.2, the cross section remains the same for all 2HDM types. In Figure 6.2 we have compared the CP-even scalars in different channels and showed that the SM-like Higgs has a higher cross-section compared to the heavy Higgs boson in both channels,

the total cross section in ep collision as a function of center of mass energy (SM-like and heavy Higgs) without any cuts. The CC process in both the SM-like and the heavy Higgs is larger than the NC process, this happens because the NC process

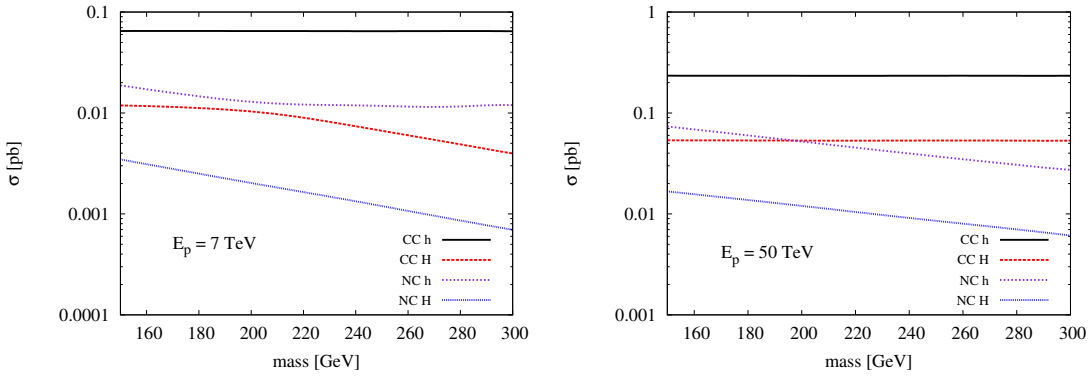

Figure 6.3: The plots shows the mass dependence of the Higgs boson, $m_{h,H}$, on the production cross section for a fixed value of energy for the incoming electron at $E_e = 60$ TeV for LHeC and FCC-he.

has a suppresed coupling due to the electrons.

The total production cross section of h and H with respect to electron beam energies by fixing proton beam energies as LHeC and FCC-he recommendations (i.e 7 and 50 TeV respectively in CC and NC processes where -80% electron polarisation is considered). The parameters are:

(a) $m_h = 125$ GeV, $m_H = 270$ GeV, $m_A = 450$ GeV, $m_{H^\pm} = 400$ GeV

(b) $\tan\beta = 1.0$, $\alpha = -0.53$ and

(c) $\lambda_1 = 0.1$, $\lambda_2 = 0.27$, $\lambda_3 = 1.1$, $\lambda_4 = -0.5$, $\lambda_5 = 0.5$

The choice of $m_H = 270$ GeV is essential [27]. This includes the Higgs boson transverse momentum, the limits on the production of di-Higgs bosons, the invariant mass of $VV(V = Z, W^\pm)$ and the results of the search for associated top-Higgs (tth) production.

It is important to mention that the $hVV(V = W^\pm, Z)$ couplings in the 2HDM is dependent on the choice of the mixing angles α and β. For example, couplings for hW^+W^-, hZZ depend on $\sin(\beta - \alpha)$, while in the case of HW^+W^-, HZZ, it is proportional to $\cos(\beta - \alpha)$ etc. Note that in the SM there is no such mixing angle dependence on such couplings. In Figure 6.2 our choice of parameters $\cos(\beta - \alpha) = \pm 0.25$ and $\sin(\beta - \alpha) = 0.97$, which can further be modified and scanned according to the constraints from the ATLAS and CMS analyses at the LHC. Here we choose these values so as to not evade the cross-section limits as given in 13 TeV data from ATLAS [67], where a search for new heavy scalar bosons into the four-lepton final state is performed by exploring the mass range.

Interestingly one of the important expectations from the LHeC/FCC-he is that we should be able to measure couplings of H with a very good signal to background ratio when compared with pp collisions. In our ongoing work we estimate the appropriate signal to background in CC and NC processes, so that we can have an idea for the level of the BR that can be accessible in these types of machines (which are highly dependent on the 2HDM parameters). For instance, from Figure 6.2 for $E_e = 60$ GeV the CC (NC), H production is about 2.2 fb (0.38 fb), which will give us about 2000 (380) H produced for $1ab^{-1}$ integrated luminosity at the LHeC.

Table 6.1: Branching ratio of h, H by considering the parameter choices as: $m_h = 125$ GeV, $m_H = 270$ GeV, $\tan\beta = 1$, $\alpha = -0.53$, $\lambda_1 = 0.1$, $\lambda_2 = 0.27$, $\lambda_3 = 1.1$, $\lambda_4 = -0.5$ and $\lambda_5 = 0.5$ for THDM Type-I. (Dominant BRs are shown in bold)

Modes	h	Modes	H
$\mathbf{b\bar{b}}$	$\mathbf{6.5 \times 10^{-1}}$	$b\bar{b}$	6.8×10^{-4}
$\tau^+\tau^-$	$\mathbf{7.0 \times 10^{-2}}$	$\tau^+\tau^-$	8.5×10^{-5}
$\mu^+\mu^-$	2.5×10^{-4}	$\mu^+\mu^-$	3.0×10^{-7}
$s\bar{s}$	2.5×10^{-4}	$s\bar{s}$	2.6×10^{-7}
$\mathbf{c\bar{c}}$	$\mathbf{3.2 \times 10^{-2}}$	$c\bar{c}$	3.3×10^{-5}
$t\bar{t}$	0.0×10^{-0}	$t\bar{t}$	8.5×10^{-7}
$\mathbf{gg}$	$\mathbf{8.5 \times 10^{-2}}$	gg	5.5×10^{-4}
$\gamma\gamma$	1.4×10^{-3}	$\gamma\gamma$	6.7×10^{-6}
$Z\gamma$	1.0×10^{-3}	$Z\gamma$	1.1×10^{-5}
$\mathbf{W^+W^-}$	$\mathbf{1.4 \times 10^{-1}}$	$\mathbf{W^+W^-}$	$\mathbf{7.1 \times 10^{-2}}$
$\mathbf{ZZ}$	$\mathbf{1.8 \times 10^{-2}}$	$\mathbf{ZZ}$	$\mathbf{3.1 \times 10^{-2}}$
		$\mathbf{hh}$	$\mathbf{9.0 \times 10^{-1}}$

Table 6.2: Branching ratio of $A, H^\pm$ by considering the parameter choices as: $m_A = 450$ GeV and $m_{H^\pm} = 400$ GeV, $\tan\beta = 1$, $\alpha = -0.53$, $\lambda_1 = 0.1$, $\lambda_2 = 0.27$, $\lambda_3 = 1.1$, $\lambda_4 = -0.5$ and $\lambda_5 = 0.5$ for THDM Type-I. (Dominant BRs are shown in bold)

Modes	A	Modes	$H^\pm$
$b\bar{b}$	2.7×10^{-4}	bc	5.9×10^{-7}
$\tau\nu$	4.6×10^{-5}		
$\mu^+\mu^-$	1.3×10^{-7}	$\mu\nu$	1.6×10^{-7}
$s\bar{s}$	9.6×10^{-8}	su	6.2×10^{-9}
$c\bar{c}$	1.4×10^{-5}	cs	1.5×10^{-5}
$\mathbf{t\bar{t}}$	$\mathbf{7.6 \times 10^{-1}}$	$\mathbf{tb}$	$\mathbf{8.7 \times 10^{-1}}$
gg	3.1×10^{-3}	cd	8.2×10^{-7}
$\gamma\gamma$	9.4×10^{-6}	bu	4.1×10^{-9}
$Z\gamma$	2.4×10^{-6}	ts	1.4×10^{-3}
$\mathbf{Zh}$	$\mathbf{5.1 \times 10^{-2}}$	td	6.5×10^{-5}
$\mathbf{ZH}$	$\mathbf{1.84 \times 10^{-1}}$	$\mathbf{hW^\pm}$	$\mathbf{4.6 \times 10^{-2}}$
W^+H^-	3.6×10^{-5}	$\mathbf{HW^\pm}$	$\mathbf{8.3 \times 10^{-2}}$

Chapter 7

Conclusion

In this chapter, we shall summarise and conclude our work and look at possible future work. The SM serves as a stepping stone, where through the Higgs mechanism, which predicts the mass of the Higgs boson, the vector bosons and fermions. Although the SM can fit the data, it has some inadequacies. It is these inadequacies that motivate us to search for BSM physics and in this dissertation, we reviewed the 2HDM which is a simple extension of the SM (where it has one additional Higgs doublet).

We continue further with the 2HDM and look at the EWSB and the results are such that there are five Higgs scalars, which can be categorised as CP-even scalars, CP-odd scalars and the charged Higgses. The CP-even scalars are split into two, the light Higgs boson (the SM-like Higgs) and the heavy scalar boson, we have considered the alignment limit for the splitting of the CP-even scalars.

We have reviewed the theoretical and experimental constraints which are important when we study the 2HDM. These constraints are the positivity of the potential and the unitarity of the scattering amplitudes. The experimental constraints are the rare decays that we can have in 2HDM, such as the $b \to s\gamma$ and the suppression of the FCNCs.

Our interest is to investigate the CP-even scalars in the possible future colliders such as the LHeC. Our starting point has been to review the production of the existing colliders such as the LHC, where we also reviewed the production of the CP-even Higgses in the ILC. According to our choice of parameters, using the Madala hypothesis, which includes the Madala boson. The introduction of the Madala hypothesis is to explain some anomalies in the Higgs data, which has been studied

quite intensively.

The cross-sectional study of the heavy Higgs boson (Madala boson) and the SM-like Higgs boson has been shown in Figure 6.2 for both CC and NC channels in LHeC and FCC-he. This shows that the heavy Higgs boson in the NC channel has been suppressed and the heavy Higgs boson in the CC channel is dominant and is closer to the SM-like Higgs boson, this means there is a higher probability of producing the heavy Higgs boson in the CC channel together with the SM-like Higgs boson in the NC channel. Comparing the two colliders, LHeC and FCC-he, we see that in the FCC-he the heavy Higgs boson in the CC channel and the SM-like Higgs boson in the NC channel have higher cross section compared to the LHeC. By increasing the energy of the collider, we have a high chance of detecting the heavy Higgs boson.

We have also studied the branching ratios of the 2HDM particle spectrum in Table 6.1-6.2. For a heavy Higgs boson, we have chosen a parameter of $m_H = 270$ GeV and the dominant decay channel is $H \to hh$. This dominant decay channel allows us to study the Madala hypothesis in details as discussed in section 3.4

There are various analyses which remain for our future studies, some of these are:

1. A full analysis of the kinematics of the final states using decays of h and H with appropriate backgrounds, and an estimation of the accuracy of the BRs in different final states, say, $b\bar{b}$, $\tau^+\tau^-$ etc.

2. A study of the dependence of the parameter space on different observables. It is important to mention here that the choice of parameter space must be consistent with all current Higgs constraints by using `HiggsSignal` and `HiggsBounds` [68]. Though the single parameter choice we took for our studies is also consistent with these constraints.

3. An exploration of the other scalars of the 2HDMs, such as the CP-odd A and the charged Higgs $H^\pm$, should be added for future studies. Note that few studies for light $H^\pm$ production and decay in e^-p environment can be found in Refs [69]

4. A consistency check with the constrained parameter space of the 2HDMs through various studies available at the LHC and e^+e^- colliders.

5. Studies related to the FCNCs, which are also very important.

Appendix A

Branching ratio

Calculating the decay rate of the Higgs to fermions, we first calculate the matrix element $|\mathcal{M}|^2$, starting with

$$\begin{aligned}
\mathcal{M} &= \frac{m_f}{\sqrt{2}v}\bar{U_{s1}}(p_1)V_{s2}(-p_2) \\
\implies \mathcal{M}^\dagger &= \frac{m_f}{\sqrt{2}v}[\bar{U_{s1}}(p_1)V_{s2}(-p_2)]^\dagger \\
&= \frac{m_f}{\sqrt{2}v}[U^\dagger_{s1}(p_1)\gamma^0 V_{s2}(-p_2)]^\dagger \\
&= \frac{m_f}{\sqrt{2}v}[U_{s1}(p_1)\gamma^{0\dagger} V^\dagger_{s2}(-p_2)] \\
&= \frac{m_f}{\sqrt{2}v}[U_{s1}(p_1)\gamma^0 V^\dagger_{s2}(-p_2)] \\
&= \frac{m_f}{\sqrt{2}v}[U_{s1}(p_1)\bar{V_{s2}}(-p_2)].
\end{aligned}$$

In Calculating the matrix elemant, we want to sum over spins:

$$
\begin{aligned}
\sum |\mathcal{M}|^2 &= \sum \mathcal{M}\mathcal{M}^\dagger \\
&= \sum [\frac{m_f}{\sqrt{2}v}\bar{U_{s1}}(p_1)V_{s2}(-p_2)\frac{m_f}{\sqrt{2}v}U_{s1}(p_1)\bar{V_{s2}}(-p_2)] \\
&= \frac{m_f^2}{2v^2}\sum [\bar{U_{s1}}(p_1)V_{s2}(-p_2)U_{s1}(p_1)\bar{V_{s2}}(-p_2)] \\
&= \frac{m_f^2}{2v^2}\sum [\bar{U_{s1}}U_{s1}(p_1)(p_1)\bar{V_{s2}}(-p_2)V_{s2}(-p_2)] \\
&= \frac{m_f^2}{2v^2}Tr[(\not{p}_1 + m_f)(-\not{p}_2 - m_f)] \\
&= \frac{m_f^2}{2v^2}Tr[-\not{p}_1 \cdot \not{p}_2 - \not{p}_1 m_f - \not{p}_2 m_f - m_f^2] \\
&= \frac{m_f^2}{2v^2}Tr[-\not{p}_1 \cdot \not{p}_2 - m_f^2] \\
&= \frac{m_f^2}{2v^2}[-Tr(\not{p}_1 \cdot \not{p}_2) - m_f^2 Tr(1)] \\
&= \frac{m_f^2}{2v^2}[-4(\not{p}_1 \cdot \not{p}_2) - 4m_f^2] \\
&= \frac{m_f^2}{2v^2}[2m_h^2 - 4m_f^2 - 4m_f^2] \\
&= \frac{m_f^2}{2v^2}[2m_h^2 - 8m_f^2] \\
&= \frac{m_f^2}{2v^2}2m_h^2\beta^2, \qquad \text{with} \qquad \beta = \sqrt{1 - \frac{4m_f^2}{m_h^2}} \\
&= \left(\frac{m_f}{v}\right)^2 m_h^2\beta^2 N_c.
\end{aligned}
$$

Therefore

$$
\begin{aligned}
\frac{d\Gamma}{d\Omega} &= \frac{|\mathcal{M}|^2}{32\pi^2 s}|p_f|s \\
d\Gamma &= \left(\frac{m_f}{v}\right)^2 \frac{m_h^2\beta^2 N_c}{32\pi^2 m_h^2}\frac{1}{2}\beta\sqrt{s}4\pi \\
\Gamma(h \to f\bar{f}) &= \frac{N_c}{8\pi v^2}m_f^2 m_h \beta^2.
\end{aligned}
$$

To show the completeness relation, we start from the Dirac's equation:

$$
\begin{aligned}
&(\not{p} - m)U(p) = 0 \\
&\bar{U}(p)(\not{p} - m) = 0 \\
\implies &\bar{U}(p)\gamma^\mu(\not{p} - m)U(p) + \bar{U}(p)(\not{p} - m)\gamma^\mu U(p) = 0 \\
\implies &\bar{U}(p)\gamma^\mu(\gamma^\alpha p_\alpha - m)U(p) + \bar{U}(p)(\gamma^\alpha p_\alpha - m)\gamma^\mu U(p) = 0 \\
\implies &\bar{U}(p)\gamma^\mu\gamma^\alpha p_\alpha U(p) - \bar{U}(p)\gamma^\mu m U(p) + \bar{U}(p)\gamma^\alpha\gamma^\mu p_\alpha U(p) - \bar{U}(p)\gamma^\alpha m U(p) = 0 \\
\implies &\bar{U}(p)\gamma^\mu\gamma^\alpha p_\alpha U(p) + \bar{U}(p)\gamma^\alpha\gamma^\mu p_\alpha U(p) - \bar{U}(p)\gamma^\mu m U(p) - \bar{U}(p)\gamma^\alpha m U(p) = 0 \\
\implies &\bar{U}(p)p_\alpha(\gamma^\mu\gamma^\alpha + \gamma^\alpha\gamma^\mu)U(p) - 2m\bar{U}(p)\gamma^\mu U(p) = 0
\end{aligned}
$$

Setting $\mu = 0$

$$
\begin{aligned}
\implies &\bar{U}(p)p_\alpha(\gamma^0\gamma^\alpha + \gamma^\alpha\gamma^0)U(p) - 2m\bar{U}(p)\gamma^0 U(p) = 0 \\
\implies &p^0\bar{U}_s(p)U_r(p) - m\bar{U}_s(p)\gamma^0 U_r(p) = 0 \\
\implies &E\bar{U}_s(p)U_r(p) - mU_s^\dagger(p)\gamma^0\gamma^0 U_r(p) = 0 \\
\implies &E\bar{U}_s(p)U_r(p) - mU_s^\dagger(p)U_r(p) = 0 \\
\implies &E\bar{U}_s(p)U_r(p) - 2mE\delta_{rs} = 0 \\
\implies &\bar{U}_s(p)U_r(p) = 2m\delta_{rs}
\end{aligned}
$$

We are required to show that:

$$\sum_s U_s(p)\bar{U}_s(p) = \not{p} + m \tag{A.1}$$

where we have that:

$$
\begin{aligned}
&\sum_s U_s(p)\bar{U}_s(p)U_r(p) \\
\implies &\sum_s U_s(p)(2m\delta_{rs}) \\
=&2mU_r(p).
\end{aligned}
$$

From Dirac's equation:

$$
\begin{aligned}
&(\not{p} + m)U_r(p) = 2mU_r(p) \\
\implies &\sum_s U_s(p)\bar{U}_s(p)U_r(p) = (\not{p} + m)U_r(p),
\end{aligned}
$$

and hence:

$$\sum_s U_s(p)\bar{U}_s(p) = (\not{p} + m). \tag{A.2}$$

Similarly:

$$\sum_s V_s(p)\bar{V}_s(p) = (-\not{p} - m). \tag{A.3}$$

Appendix B

Parton distribution functions

The PDFs is a probability for a parton to carry the fraction x of a proton's momentum, as shown in Figure B. The PDFs are of crucial importance for precision physics at colliders, because they limit the accuracy of the SM predictions including the Higgs boson. They reach new physics searches at high Bjorken x. The PDFs determination is based on QCD factorisation, where the observable cross-section $\sigma(x, Q^2)$ can be measured experimentally, and where the Q^2 dependence of the σ is given in perturbative QCD. Note that the x-dependence is not calculable in perturbative QCD.

The understanding of the structure of the proton at short distances is one of the key ingredients to be able to predict the cross-section for processes involving hadrons in the initial state. All processes in hadronic collisions, even those intrinsically of electroweak nature (such as the production of W/Z bosons or photons), are in fact induced by quarks and gluons contained inside the hadron.

The most accurate available information on the PDFs of the protons, as essential ingredients for hadron collider phenomenology, comes from global fits to extended sets of data obtained from a variety of different electro and hadroproduction processes, in particular, DIS, Drell-Yan, gauge boson production and jet production. The combination of the information from all these processes allows one to determine six independent light quark and antiquark distributions and gluons. Data from the LHC are likely to offer very significant improvements in the accuracy of these determinations.

The PDFs are most precisely determined from DIS data. However, DIS structure functions probe only particular combinations of PDFs, DIS data leads to a very pre-

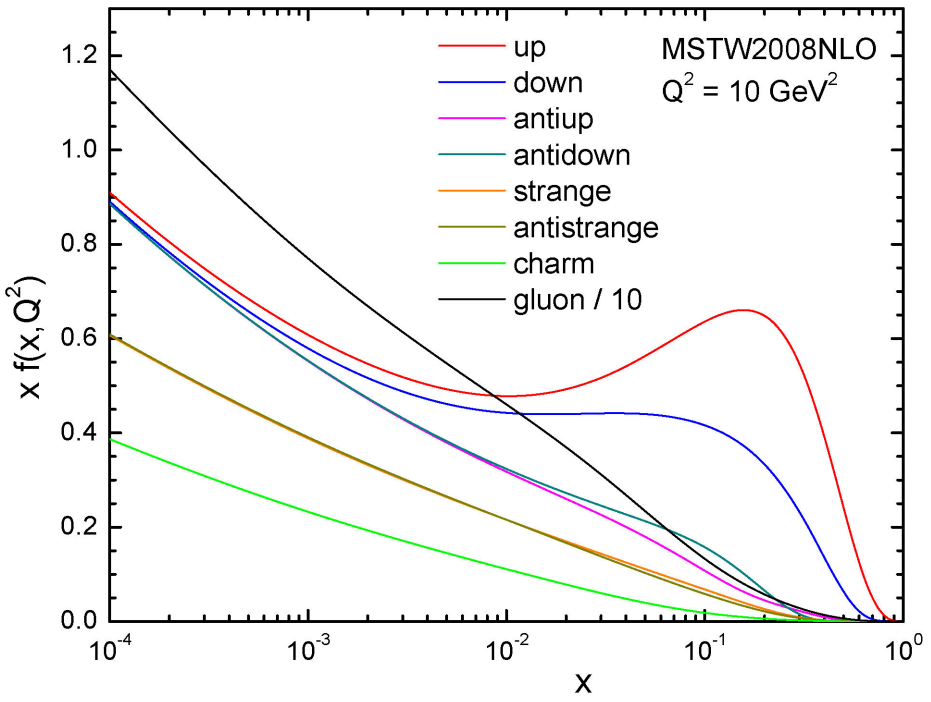

Figure B.1: Parton Density of proton

cise determination of valence PDFs. The cross-section measurements at the hadron collider cannot replace the invaluable DIS data, nevertheless they can provide important complementary imformation in the orders of the phase space not well covered by other datasets.

Appendix C

Scattering Amplitude

We first start by writing down the Feynman rules shown in Figure C in order to compute the matrix element of any process,

- Incoming electron : $U^{(s_1)}(p_1)$
- Outgoing electron : $\bar{U}^{(s_3)}(p_3)$
- Electron-electron vertex : $ig_e\gamma^\mu$
- Internal photon : $-\frac{ig_{\mu\nu}}{q^2}$
- Incoming muon : $U^{(s_2)}(p_2)$
- Outgoing muon : $\bar{U}^{(s_4)}(p_4)$
- muon-muon vertex : $ig_e\gamma^\nu$
- Delta funtion at the electron-electron vertex :$(2\pi)^4\delta^4(p_1 - p_3 - q)$
- Delta function at the muon-muon vertex :$(2\pi)^4\delta^4(p_2 - p_4 + q)$
- Internal momentum q : $\frac{d^4q}{(2\pi)^4}$

We combine all these factors together and we get

$$(2\pi)^4 \int [\bar{U}^{(s_3)}(p_3)(ig_e\gamma^\mu)U^{(s_1)}(p_1)]$$
$$-\frac{ig_{\mu\nu}}{q^2}[\bar{U}^{(s_4)}(p_4)(ig_e\gamma^\nu)U^{(s_2)}(p_2)](2\pi)^4\delta^4(p_1 - p_3 - q)(2\pi)^4\delta^4(p_2 - p_4 + q)d^4q.$$

Dropping the delta functions and equating it to $-i\mathcal{M}$:

$$-i\mathcal{M} = \frac{ig_e^2}{(p_1 - p_3)}[\bar{u}^{s_3}(p_3)\gamma^\mu u^{s_1}(p_1)][\bar{u}^{s_4}(p_4)\gamma_\mu u^{s_2}(p_2)] \tag{C.1}$$

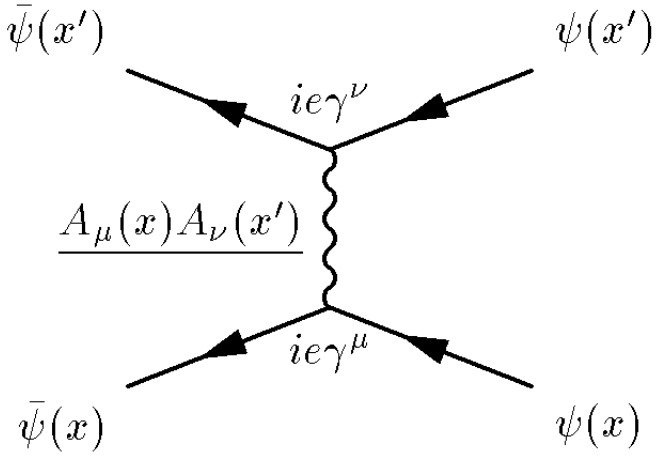

Figure C.1: Feynman diagram for electron-electron scattering.

To determine the amplitude we have to square both sides,

$$|\mathcal{M}|^2 = \frac{ig_e^2}{(p_1 - p_3)}[\bar{u}^{s_3}(p_3)\gamma^{\mu}u^{s_1}(p_1)][\bar{u}^{s_4}(p_4)\gamma_{\mu}u^{s_2}(p_2)] \tag{C.2}$$
$$\times[\bar{u}^{s_3}(p_3)\gamma^{\nu}u^{s_1}(p_1)]^*[\bar{u}^{s_4}(p_4)\gamma_{\nu}u^{s_2}(p_2)]^*$$

To calculate the complex conjugate terms we should use the Casmir trick []. To calculate the amplitude we should average over the initial spins and sum over the final spins. Hence we would replace $|\mathcal{M}|^2$ with $\langle|\mathcal{M}|^2\rangle$.

Let:

$$G = [\bar{u}(a)\Gamma_1 u(b)][\bar{u}(a)\Gamma_2 u(b)]^*. \tag{C.3}$$

Evaluating the complex conjugate:

$$\begin{aligned}[\bar{u}(a)\Gamma_2 u(b)]^* &= [u(a)^{\dagger}\gamma^0\Gamma_2 u(b)]^{\dagger} \\ &= u(b)^{\dagger}\Gamma_2^{\dagger}u(a) \\ &= u(b)^{\dagger}\gamma^0\gamma^0\Gamma_2^{\dagger}\gamma^0 u(a) \\ &= \bar{u}(b)\bar{\Gamma}_2 u(a).\end{aligned}$$

Therefore

$$G = [\bar{u}(a)\Gamma_1 u(b)][\bar{u}(b)\bar{\Gamma}_2 u(a)]. \tag{C.4}$$

Summing over the spin orientation of particle b :

$$\begin{aligned}\sum_{bspins} G &= \bar{u}(a)\Gamma_1\left[\sum_{s_a=1,2} u^{(s_b)}(p_b)\bar{u}^{(s_b)(p_b)}\right]\bar{\Gamma}_2 u(a)\\ &= \bar{u}(a)\Gamma_1(\not{p}_b + m_b c)\bar{\Gamma}_2 u(a)\\ &= \bar{u}(a)Qu(a),\end{aligned}$$

where we note that

$$\begin{aligned}&\sum_s U_s(p)\bar{U}_s(p) = \not{p} + m\\ &\text{with } \not{p}_b = \gamma^\mu p_\mu, \text{and}\\ &Q = \Gamma_1(\not{p}_b + m_b c)\bar{\Gamma}_2.\end{aligned}$$

Summing over the spin orientation of particle a :

$$\begin{aligned}\sum_{aspins}\sum_{bspins} G &= \sum_{s_a=1,2} \bar{u}_i^{(s_a)}(p_a)Q_{ij}u^{(s_a)}(p_a)_j\\ &= Q_{ij}\left[\bar{u}^{(s_a)}(p_a)u^{(s_a)}(p_a)\right]_{ji}\\ &= Q_{ij}(\not{p}_a + m_a c)_{ji}\\ &= Tr(Q(\not{p}_a + m_a c)).\end{aligned}$$

Thus for our final result is:

$$\sum_{allspins}[\bar{u}(a)\Gamma_1 u(b)][\bar{u}(a)\Gamma_2 u(b)]^* = Tr[\Gamma_1(\not{p}_b + m_b c)\bar{\Gamma}_2(\not{p}_a m_a c)]. \tag{C.5}$$

Applying the Casimir trick twice, we obtain the average for our electron-proton scattering amplitude:

$$\langle|\mathcal{M}|^2\rangle = \frac{g^4}{4(p_1 - p_3)^4}Tr[\gamma^\mu(\not{p}_1 + m_e c)\gamma^\nu(\not{p}_3 + m_e c)]Tr[\gamma_\mu(\not{p}_2 + m_p c)\gamma_\nu(\not{p}_4 + m_p c)]. \tag{C.6}$$

Simplifying the traces we get the following, where we have used the trace theorems:

$$\begin{aligned}Tr[\gamma^\mu(\not{p}_1 + m_e c)\gamma^\nu(\not{p}_3 + m_e c)] &= Tr(\gamma^\mu\not{p}_1\gamma^\nu\not{p}_3) + m_e c[Tr(\gamma^\mu\not{p}_1\gamma^\nu)\\ &\quad + Tr(\gamma^\mu)\gamma^\nu\not{p}_3] + (m_e c)^2 Tr(\gamma^\mu\gamma^\nu)\end{aligned} \tag{C.7}$$

We only evaluate the first term, the second term vanishes and the last term is given by $4g^{\mu\nu}$:

$$Tr(\gamma^\mu \not{p}_1 \gamma^\nu \not{p}_3) = (p_1)_\lambda (p_3)_\sigma Tr(\gamma^\mu \gamma^\lambda \gamma^\nu \gamma^\sigma) \tag{C.8}$$

$$= (p_1)_\lambda (p_3)_\sigma 4(g^{\mu\lambda} g^{\nu\sigma} - g^{\mu\nu} g^{\lambda\sigma} + g^{\mu\sigma} g^{\lambda\nu}) \tag{C.9}$$

$$= 4[p_1^\mu p_3^\nu - g^{\mu\nu}(p_1 \cdot p_3) + p_3^\mu p_1^\nu]. \tag{C.10}$$

Therefore

$$Tr[\gamma^\mu(\not{p}_1 + m_e c)\gamma^\nu(\not{p}_3 + m_e c)] = 4[p_1^\mu p_3^\nu - g^{\mu\nu}(m_e^2 c^2 - p_1 \cdot p_3) + p_3^\mu p_1^\nu] \tag{C.11}$$

We apply the same procedure for the proton:

$$Tr[\gamma^\mu(\not{p}_2 + m_p c)\gamma^\nu(\not{p}_4 + m_p c)] = 4[p_2^\mu p_4^\nu - g^{\mu\nu}(m_p^2 c^2 - p_2 \cdot p_4) + p_4^\mu p_2^\nu] \tag{C.12}$$

Substituting Eqn. C.11 and Eqn. C12 into Eqn. C.6

$$\langle |\mathcal{M}|^2 \rangle = \frac{4g^4}{4(p_1 - p_3)^4}[p_1^\mu p_3^\nu - g^{\mu\nu}(m_e^2 c^2 - p_1 \cdot p_3) + p_3^\mu p_1^\nu] \tag{C.13}$$

$$\times [p_2^\mu p_4^\nu - g^{\mu\nu}(m_p^2 c^2 - p_2 \cdot p_4) + p_4^\mu p_2^\nu]$$

$$= \frac{8g^4}{4(p_1 - p_3)^4}[(p_1 \cdot p_2)(p_3 \cdot p_4) + (p_1 \cdot p_4)(p_2 \cdot p_3) - (p_1 \cdot p_3)(m_p^2 c^2)$$

$$- (p_2 \cdot p_4)(m_e c)^2 - 2(m_e m_p c^2)^2] \tag{C.14}$$

$$\langle |\mathcal{M}_{fi}|^2 \rangle = \frac{8g^4}{(p_1 - p_3)^4}\Big[(p_1 \cdot p_2)(p_3 \cdot p_4) + (p_1 \cdot p_4)(p_2 \cdot p_3) - (p_1 \cdot p_3)m_p^2\Big]. \tag{C.15}$$

Bibliography

[1] C. Mosomane, M. Kumar, A. S. Cornell, and B. Mellado, *Exploring CP-even scalars of a Two Higgs-doublet model in future e^- p colliders*, J. Phys. Conf. Ser. **889** (2017) 012004, arXiv:1707.05997 [hep-ph].

[2] S. M. Bilenky and J. Hosek, *GLASHOW-WEINBERG-SALAM THEORY OF ELECTROWEAK INTERACTIONS AND THE NEUTRAL CURRENTS*, Phys. Rept. **90** (1982) 73–157.

[3] CMS Collaboration, S. Chatrchyan et al., *Observation of a new boson at a mass of 125 GeV with the CMS experiment at the LHC*, Phys. Lett. **B716** (2012) 30–61, arXiv:1207.7235 [hep-ex].

[4] J. Ellis, *Physics Beyond the Standard Model*, Nucl. Phys. **A827** (2009) 187C–198C, arXiv:0902.0357 [hep-ph], [,187(2009)].

[5] D. M. Asner et al., *ILC Higgs White Paper*, in *Proceedings, 2013 Community Summer Study on the Future of U.S. Particle Physics: Snowmass on the Mississippi (CSS2013): Minneapolis, MN, USA, July 29-August 6, 2013*. 2013. arXiv:1310.0763 [hep-ph]. https://inspirehep.net/record/1256491/files/arXiv:1310.0763.pdf.

[6] G. C. Branco, P. M. Ferreira, L. Lavoura, M. N. Rebelo, M. Sher, and J. P. Silva, *Theory and phenomenology of two-Higgs-doublet models*, Phys. Rept. **516** (2012) 1–102, arXiv:1106.0034 [hep-ph].

[7] D. H. Oaknin and A. Zhitnitsky, *Baryon asymmetry, dark matter and quantum chromodynamics*, Phys. Rev. **D71** (2005) 023519, arXiv:hep-ph/0309086 [hep-ph].

[8] M. Kumar, S. von Buddenbrock, N. Chakrabarty, A. S. Cornell, D. Kar, T. Mandal, B. Mellado, B. Mukhopadhyaya, and R. G. Reed, *The impact of additional scalar bosons at the LHC*, J. Phys. Conf. Ser. **802** (2017) 012007, arXiv:1603.01208 [hep-ph].

[9] ATLAS Collaboration, G. Aad et al., *Observation of a new particle in the search for the Standard Model Higgs boson with the ATLAS detector at the LHC*, Phys. Lett. **B716** (2012) 1–29, arXiv:1207.7214 [hep-ex].

[10] D0 Collaboration, O. Brandt, *Direct measurement of the top quark mass in $p\bar{p}$ collisions at D0*, 2017. arXiv:1710.04266 [hep-ex]. http://inspirehep.net/record/1630463/files/arXiv:1710.04266.pdf.

[11] T. Yanagisawa, *NambuâĂŞGoldstone Bosons Characterized by the Order Parameter in Spontaneous Symmetry Breaking*, J. Phys. Soc. Jap. **86** (2017) 104711.

[12] G. E. Volovik and M. A. Zubkov, *Higgs bosons in particle physics and in condensed matter*, J. Low Temp. Phys. **175** (2013) 486–497, arXiv:1305.7219 [hep-ph], [J. Low. Temp. Phys.175,486(2014)].

[13] J. F. Gunion, H. E. Haber, G. L. Kane, and S. Dawson, *The Higgs Hunter's Guide*, Front. Phys. **80** (2000) 1–404.

[14] H. E. Logan, *TASI 2013 lectures on Higgs physics within and beyond the Standard Model*, arXiv:1406.1786 [hep-ph].

[15] P. Ramond, *The Five Instructions*, pp. , 1–37. 2013. arXiv:1201.0396 [hep-ph]. https://inspirehep.net/record/1083347/files/arXiv:1201.0396.pdf.

[16] Z. Ligeti, *TASI Lectures on Flavor Physics*, pp. , 297–340. 2015. arXiv:1502.01372 [hep-ph]. https://inspirehep.net/record/1343118/files/arXiv:1502.01372.pdf.

[17] L. Canetti, M. Drewes, and M. Shaposhnikov, *Matter and Antimatter in the Universe*, New J. Phys. **14** (2012) 095012, arXiv:1204.4186 [hep-ph].

[18] C. Giganti, S. Lavignac, and M. Zito, *Neutrino oscillations: the rise of the PMNS paradigm*, Prog. Part. Nucl. Phys. **98** (2018) 1–54, arXiv:1710.00715 [hep-ex].

[19] S. Capozziello, L. Consiglio, M. De Laurentis, G. De Rosa, and C. Di Donato, *The missing matter problem: from the dark matter search to alternative hypotheses*, arXiv:1110.5026 [astro-ph.CO].

[20] CMS Collaboration, V. Khachatryan et al., *Search for neutral resonances decaying into a Z boson and a pair of b jets or τ leptons*, Phys. Lett. **B759** (2016) 369–394, arXiv:1603.02991 [hep-ex].

[21] J. Bernon, J. F. Gunion, H. E. Haber, Y. Jiang, and S. Kraml, *Scrutinizing the alignment limit in two-Higgs-doublet models: m_h=125âĂĽâĂĽGeV*, Phys. Rev. **D92** (2015) 075004, arXiv:1507.00933 [hep-ph].

[22] J. Bernon, J. F. Gunion, H. E. Haber, Y. Jiang, and S. Kraml, *Scrutinizing the alignment limit in two-Higgs-doublet models. II. m_H=125âĂĽâĂĽGeV*, Phys. Rev. **D93** (2016) 035027, arXiv:1511.03682 [hep-ph].

[23] A. Crivellin, A. Kokulu, and C. Greub, *Flavor-phenomenology of two-Higgs-doublet models with generic Yukawa structure*, Phys. Rev. **D87** (2013) 094031, arXiv:1303.5877 [hep-ph].

[24] G. Cree and H. E. Logan, *Yukawa alignment from natural flavor conservation*, Phys. Rev. **D84** (2011) 055021, arXiv:1106.4039 [hep-ph].

[25] S. Kanemura, T. Kubota, and E. Takasugi, *Lee-Quigg-Thacker bounds for Higgs boson masses in a two doublet model*, Phys. Lett. **B313** (1993) 155–160, arXiv:hep-ph/9303263 [hep-ph].

[26] A. Djouadi, J. Kalinowski, and M. Spira, *HDECAY: A Program for Higgs boson decays in the standard model and its supersymmetric extension*, Comput. Phys. Commun. **108** (1998) 56–74, arXiv:hep-ph/9704448 [hep-ph].

[27] S. von Buddenbrock, N. Chakrabarty, A. S. Cornell, D. Kar, M. Kumar, T. Mandal, B. Mellado, B. Mukhopadhyaya, and R. G. Reed, *The compatibility of LHC Run 1 data with a heavy scalar of mass around 270 GeV*, arXiv:1506.00612 [hep-ph].

[28] S. von Buddenbrock, *Exploring LHC Run 1 and 2 data using the Madala hypothesis*, J. Phys. Conf. Ser. **878** (2017) 012030, arXiv:1706.02477 [hep-ph].

[29] M. Kumar, S. von Buddenbrock, N. Chakrabarty, A. S. Cornell, D. Kar, T. Mandal, B. Mellado, B. Mukhopadhyaya, R. G. Reed, and X. Ruan, *Phenomenology of additional scalar bosons at the LHC*, in *61st Annual Conference of the South African Institute of Physics (SAIP2016) Johannesburg, South Africa, July 4-8, 2016*. 2016. arXiv:1608.03466 [hep-ph].
https://inspirehep.net/record/1480869/files/arXiv:1608.03466.pdf.

[30] S. von Buddenbrock, N. Chakrabarty, A. S. Cornell, D. Kar, M. Kumar, T. Mandal, B. Mellado, B. Mukhopadhyaya, R. G. Reed, and X. Ruan,

Phenomenological signatures of additional scalar bosons at the LHC, Eur. Phys. J. **C76** (2016) 580, arXiv:1606.01674 [hep-ph].

[31] P. M. Ferreira and D. R. T. Jones, *Bounds on scalar masses in two Higgs doublet models*, JHEP **08** (2009) 069, arXiv:0903.2856 [hep-ph].

[32] S. Sultansoy, *A Review of TeV scale lepton-hadron and photon-hadron colliders*, Conf. Proc. **C0505161** (2005) 4329, arXiv:hep-ex/0508020 [hep-ex], [,4329(2005)].

[33] I. F. Ginzburg and I. P. Ivanov, *Tree-level unitarity constraints in the most general 2HDM*, Phys. Rev. **D72** (2005) 115010, arXiv:hep-ph/0508020 [hep-ph].

[34] M. Ciuchini, E. Franco, G. Martinelli, L. Reina, and L. Silvestrini, *Scheme independence of the effective Hamiltonian for b —¿ s gamma and b —¿ s g decays*, Phys. Lett. **B316** (1993) 127–136, arXiv:hep-ph/9307364 [hep-ph].

[35] A. J. Buras, M. Misiak, M. Munz, and S. Pokorski, *Theoretical uncertainties and phenomenological aspects of B —¿ X(s) gamma decay*, Nucl. Phys. **B424** (1994) 374–398, arXiv:hep-ph/9311345 [hep-ph].

[36] A. Wahab El Kaffas, P. Osland, and O. M. Ogreid, *Constraining the Two-Higgs-Doublet-Model parameter space*, Phys. Rev. **D76** (2007) 095001, arXiv:0706.2997 [hep-ph].

[37] A. Arbey, F. Mahmoudi, O. Stal, and T. Stefaniak, *Status of the Charged Higgs Boson in Two Higgs Doublet Models*, arXiv:1706.07414 [hep-ph].

[38] A. G. Holzner, *Searches for charged Higgs bosons at LEP*, in *36th Rencontres de Moriond on Electroweak Interactions and Unified Theories Les Arcs, France, March 10-17, 2001*. 2001. arXiv:hep-ex/0105045 [hep-ex].

[39] M. Hussain, M. Usman, M. A. Paracha, and M. J. Aslam, *Constraints on Two Higgs Doublet Model Parameters in the light of rare B-Decays*, Phys. Rev. **D95** (2017) 075009, arXiv:1703.10845 [hep-ph].

[40] J. Hernandez-Sanchez, S. P. Das, S. Moretti, A. Rosado, and R. Xoxocotzi-Aguilar, *Flavor violating signatures of neutral Higgs bosons at the LHeC*, PoS **DIS2015** (2015) 227, arXiv:1509.05491 [hep-ph].

[41] K. Kumericki, *Feynman Diagrams for Beginners*, 2016. arXiv:1602.04182 [physics.ed-ph].
http://inspirehep.net/record/1478654/files/arXiv:1602.04182.pdf.

[42] CMS Collaboration, V. Khachatryan et al., *Transverse momentum and pseudorapidity distributions of charged hadrons in pp collisions at* $\sqrt{s} = 0.9$ *and 2.36 TeV*, JHEP **02** (2010) 041, arXiv:1002.0621 [hep-ex].

[43] A. Ballestrero, E. Maina, and G. Pelliccioli, *W boson polarization in vector boson scattering at the LHC*, arXiv:1710.09339 [hep-ph].

[44] B. Bhattacherjee, A. Choudhury, K. Ghosh, and S. Poddar, *Compressed supersymmetry at 14 TeV LHC*, Phys. Rev. **D89** (2014) 037702, arXiv:1308.1526 [hep-ph].

[45] D. Ghosh, R. Godbole, M. Guchait, K. Mohan, and D. Sengupta, *Looking for an Invisible Higgs Signal at the LHC*, Phys. Lett. **B725** (2013) 344–351, arXiv:1211.7015 [hep-ph].

[46] A. Alves, D. A. Camargo, and A. G. Dias, *Heavy Higgs boson coupled to vectorlike quarks: Strong CP problem and search prospects at the 14 TeV LHC*, Phys. Rev. **D94** (2016) 015027, arXiv:1511.04449 [hep-ph], [Addendum: Phys. Rev.D94,no.5,059901(2016)].

[47] B. Dumont, J. F. Gunion, Y. Jiang, and S. Kraml, *Constraints on and future prospects for Two-Higgs-Doublet Models in light of the LHC Higgs signal*, Phys. Rev. **D90** (2014) 035021, arXiv:1405.3584 [hep-ph].

[48] CMS Collaboration, V. Khachatryan et al., *Searches for heavy Higgs bosons in two-Higgs-doublet models and for tâĘŠch decay using multilepton and diphoton final states in pp collisions at 8 TeV*, Phys. Rev. **D90** (2014) 112013, arXiv:1410.2751 [hep-ex].

[49] T. Behnke, J. E. Brau, B. Foster, J. Fuster, M. Harrison, J. M. Paterson, M. Peskin, M. Stanitzki, N. Walker, and H. Yamamoto, *The International Linear Collider Technical Design Report - Volume 1: Executive Summary*, arXiv:1306.6327 [physics.acc-ph].

[50] K. Fujii et al., *Physics Case for the International Linear Collider*, arXiv:1506.05992 [hep-ex].

[51] S. Abeyratne et al., *Science Requirements and Conceptual Design for a Polarized Medium Energy Electron-Ion Collider at Jefferson Lab*, arXiv:1209.0757 [physics.acc-ph].

[52] LHeC Study Group Collaboration, J. L. Abelleira Fernandez et al., *A Large Hadron Electron Collider at CERN: Report on the Physics and Design*

Concepts for Machine and Detector, J. Phys. **G39** (2012) 075001, arXiv:1206.2913 [physics.acc-ph].

[53] B. Coleppa, M. Kumar, S. Kumar, and B. Mellado, *Measuring CP nature of top-Higgs couplings at the future Large Hadron electron collider*, Phys. Lett. **B770** (2017) 335–341, arXiv:1702.03426 [hep-ph].

[54] O. Bruening and M. Klein, *The Large Hadron Electron Collider*, Mod. Phys. Lett. **A28** (2013) 1330011, arXiv:1305.2090 [physics.acc-ph].

[55] R. Talman, *Scaling Behavior of Circular Colliders Dominated by Synchrotron Radiation*, Int. J. Mod. Phys. **A30** (2015) 1544003, arXiv:1504.01627 [physics.acc-ph].

[56] X. Wang, H. Sun, and X. Luo, *Searches for the Anomalous FCNC Top-Higgs Couplings with Polarized Electron Beam at the LHeC*, Adv. High Energy Phys. **2017** (2017) 4693213, arXiv:1703.02691 [hep-ph].

[57] D. d'Enterria, α_s *review (2016)*, pp. , 91–96. 2016. arXiv:1606.04772 [hep-ph].
https://inspirehep.net/record/1469451/files/arXiv:1606.04772.pdf.

[58] J. B. Dainton, M. Klein, P. Newman, E. Perez, and F. Willeke, *Deep inelastic electron-nucleon scattering at the LHC*, JINST **1** (2006) P10001, arXiv:hep-ex/0603016 [hep-ex].

[59] M. Klein and R. Yoshida, *Collider Physics at HERA*, Prog. Part. Nucl. Phys. **61** (2008) 343–393, arXiv:0805.3334 [hep-ex].

[60] M. Klein, *Future Deep Inelastic Scattering with the LHeC*, arXiv:1802.04317 [hep-ph].

[61] A. V. Gramolin and D. M. Nikolenko, *Reanalysis of Rosenbluth measurements of the proton form factors*, Phys. Rev. **C93** (2016) 055201, arXiv:1603.06920 [nucl-ex].

[62] P. Kostka, A. Polini, and D. M. South, *The LHeC Detector*, PoS **DIS2013** (2013) 256, arXiv:1308.6241 [physics.acc-ph].

[63] W. Zhe, W. Shao-Ming, M. Wen-Gan, G. Lei, and Z. Ren-You, *The Light MSSM neutral Higgs boson production associated with an electron and a jet at the LHeC*, Phys. Rev. **D83** (2011) 055003, arXiv:1101.4987 [hep-ph].

[64] F. Borzumati and A. Djouadi, *Lower bounds on charged Higgs bosons from LEP and Tevatron*, Phys. Lett. **B549** (2002) 170–176, arXiv:hep-ph/9806301 [hep-ph].

[65] H. Ito, O. Jinnouchi, T. Moroi, N. Nagata, and H. Otono, *Searching for Metastable Particles with Sub-Millimeter Displaced Vertices at Hadron Colliders*, arXiv:1803.00234 [hep-ph].

[66] M. Kumar, X. Ruan, A. S. Cornell, R. Islam, and B. Mellado, *Double Higgs production at FCC-he and prospects for measurements of self-coupling*, J. Phys. Conf. Ser. **623** (2015) 012017.

[67] ATLAS Collaboration, M. Aaboud et al., *Search for new high-mass phenomena in the dilepton final state using 36.1 fb^{-1} of proton-proton collision data at $\sqrt{s}$ = 13 TeV with the ATLAS detector*, arXiv:1707.02424 [hep-ex].

[68] P. Bechtle, O. Brein, S. Heinemeyer, G. Weiglein, and K. E. Williams, *HiggsBounds 2.0.0: Confronting Neutral and Charged Higgs Sector Predictions with Exclusion Bounds from LEP and the Tevatron*, Comput. Phys. Commun. **182** (2011) 2605–2631, arXiv:1102.1898 [hep-ph].

[69] S. Moretti and K. Odagiri, *Charged Higgs scalar production in single top mode (and other) at future ep colliders in the minimal supersymmetric standard model*, Phys. Rev. **D57** (1998) 5773–5779, arXiv:hep-ph/9709458 [hep-ph].